ORIGINAL PAPER

Subject-specific Model Estimation of Cardiac Output and Blood Volume During Hemorrhage

Maxwell Lewis Neal · James B. Bassingthwaighte

Abstract We have developed a novel method for estimating subject-specific hemodynamics during hemorrhage. First, a mathematical model representing a closed-loop circulation and baroreceptor feedback system was parameterized to match the baseline physiology of individual experimental subjects by fitting model results to 1 min of pre-injury data. This automated parameterization process matched pre-injury measurements within 1.4 ± 1.3% SD. Tuned parameters were then used in similar open-loop models to simulate dynamics post-injury. Cardiac output (CO) estimates were obtained continuously using post-injury measurements of arterial blood pressure (ABP) and heart rate (HR) as inputs to the first open-loop model. Secondarily, total blood volume (TBV) estimates were obtained by summing the blood volumes in all the circulatory segments of a second open-loop model that used measured CO as an additional input. We validated the estimation method by comparing model CO results to flowprobe measurements in 14 pigs. Overall, CO estimates had a Bland-Altman bias of −0.30 l/min with upper and lower limits of agreement 0.80 and −1.40 l/min. The negative bias is likely due to overestimation of the peripheral resistance response to hemorrhage. There was no reference measurement of TBV; however, the estimates appeared reasonable and clearly predicted survival versus death during the post-hemorrhage period. Both open-loop models ran in real time on a computer with a 2.4 GHz processor, and their clinical applicability in emergency care scenarios is discussed.

Keywords Computer simulation · Physiologic monitoring · Hemorrhage · Cardiac output · Blood volume

Introduction

In an effort to explore the potential clinical applications of computational physiological modeling, we developed a novel, model-based approach for estimating subject-specific hemodynamics during acute hemorrhage. Our strategy was to first tune the parameters of a closed-loop cardiovascular model so that model results matched a set of baseline (pre-injury) cardiovascular measurements for each individual study subject (pig). Then, the tuned parameters from the baseline model were loaded into similar open-loop circulatory models (diagrammed in Fig. 1) that provided post-injury hemodynamic estimates from a subset of the initial measurements. The open-loop model presented in detail here used beat-by-beat measure of heart rate (HR) and arterial blood pressure (ABP) as inputs in order to solve for all remaining model variables.

We assessed the accuracy of our estimation method by comparing model estimates of cardiac output (CO) to CO recorded with flowmeters on 14 female pigs during hemorrhage. Total blood volume (TBV) estimates, described in a second part of the study, were also evaluated, because it was hypothesized they might provide a means of predicting survival following injury. Although our models can provide many surrogate cardiovascular measurements, our focus here was on CO and TBV, since they have primary

M. L. Neal
Department of Medical Education and Biomedical Informatics, University of Washington, Seattle, WA 98195, USA
e-mail: mneal@u.washington.edu

J. B. Bassingthwaighte (✉)
Department of Bioengineering, University of Washington, 1705 NE Pacific St., Box 355061, Seattle, WA 98195-5061, USA
e-mail: jbb@bioeng.washington.edu
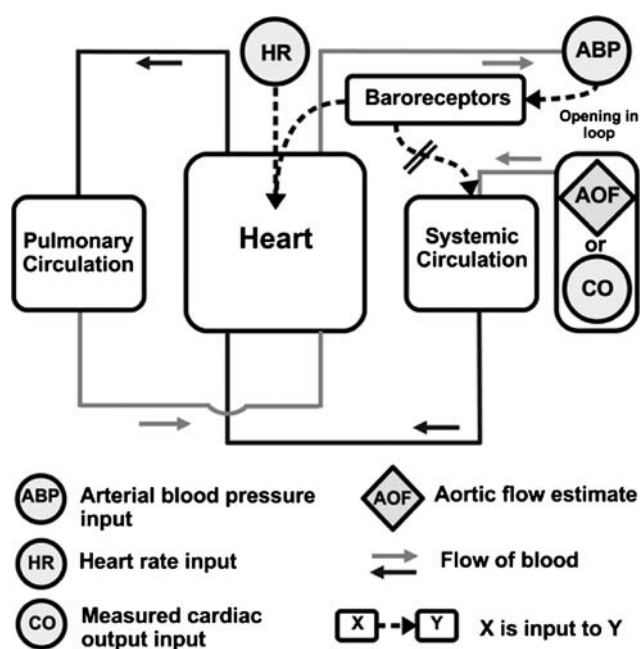
Fig. 1 Block diagram of the open-loop models used to estimate cardiac output and total blood volume. The cardiac output estimation model uses heart rate and arterial blood pressure as inputs and generates a nonpulsatile aortic flow estimate that sets the overall cardiac output estimate. The total blood volume estimation model uses heart rate, arterial blood pressure and measured cardiac output as inputs, and does not use the baroreceptor functions to set peripheral resistance in the systemic circulation (double slashes). See Model Description for details

influence on the dynamics of the circulatory model and are clinically useful in assessing injury severity.

Our method offers a means of estimating CO from HR and ABP, and therefore is a member of the family of computational techniques that derive CO and/or stroke volume from HR and ABP data. These techniques were developed in order to characterize and monitor patient status and to assist in the selection of interventions (Bourgeois et al. 1976; Kouchoukos et al. 1970; Linton and Linton 2001; McCombie et al. 2005; Redling and Akay 1997; Romano and Pistolesi 2002; Saeed and Mark 2000; Warner et al. 1953; Wesseling et al. 1993), and many rely on mathematical analysis of the ABP waveform's pulse contour to compute CO. We propose our method as an advancement over such pulse contour techniques because only relatively low-resolution data available from finger pulse detectors or blood pressure cuffs are required for model solutions.

Computational models used for CO estimation in several of the studies cited above were simplified and had limited detail. Although computational power has increased to the point where the use of more detailed circulatory systems can be considered for clinical applications, model simplicity is still necessary to reduce memory requirements and

ensure computational timeliness. The models developed for this study were all derived from a more complicated model available on our website at http://www.physiome.org/redirect/HIHwIindex.html, but not yet published with peer review. The simplified system used here contains the following components: a four-chambered heart (Heldt et al. 2001; Rideout 1991), systemic circulation (Olansen et al. 2000), pulmonary circulation (Olansen et al. 2000), coronary circulation (Zinemanas et al. 1994), and baroreceptor influence on cardiac contractility, peripheral resistance, and peripheral vasomotor tone (Lu et al. 2001). All parameter values for the CO estimation model, along with parameter and variable definitions, have been tabulated in the *Model description* section below so that the system can be reproduced from the present paper alone. To this same end, all model equations have been included in the *Appendix* and a detailed description of the automated procedure for tuning the closed-loop cardiovascular model is provided. In addition, the CO estimation model is made freely available for web operation or download at http://www.nsr.bioeng.washington.edu/PLN/Members/mneal/COest/document_vi.

Medical emergency personnel, intensive care units and surgical suites are increasingly well equipped with data acquisition and analysis capabilities and display devices. In the spirit of this advancing capability, our study demonstrates an application for the on-line calculation and display of physiological information in a situation where unobserved measurements are estimated from a few observables and patient-specific data collected prior to injury. Given that the models developed for this study can provide real time post-injury results on a 2.4 GHz desktop computer, we envision their eventual incorporation with next-generation, digital triage methods under development (Gao et al. 2006; Massey et al. 2006; Gao et al. 2005; Killeen et al. 2006; Chan et al. 2004; Gao 2006) in order to provide first responders with more powerful means of characterizing and monitoring patient-specific hemodynamics following trauma. Conceivably, if HR and ABP data are collected from a trauma patient, and the patient's baseline model parameters are accessible, our method could be used to generate a complete hemodynamic profile of that individual in real-time.

The long-range goal of this type of research is to develop models for assistance in assessment of injury, and monitoring and control of patient status in a variety of emergency care situations. Meeting this goal will require the use of reliable detection methods, computer decision-making, and inevitably, redundancy in computational hardware and software for robust operation. Our first step here, however, is to demonstrate the development and utility of a model-based, hemodynamic estimation method dependent only on measured ABP and HR.

Table 1 Measurements recorded during hemorrhage experiment

Measurement	Abbreviation	Measurement site	Recording instrument	Units
Aortic flow	AOF	Ascending aorta	Flow probe (Transonic Systems, Ithaca, NY)	l/min
Pulmonary artery flow	PAF	Pulmonary artery trunk	Flow probe (Transonic Systems, Ithaca, NY)	l/min
Arterial blood pressure	ABP	Carotid artery	Tygon catheter	mmHg
Central venous pressure	CVP	Jugular vein	Tygon catheter	mmHg
Left ventricle pressure	LVP	Left ventricle	Tygon catheter	mmHg
Right ventricle pressure	RVP	Right ventricle	Tygon catheter	mmHg
Heart rate	HR	Limbs and chest (six lead ECG)	Resampled data from ECG	min^{-1}

Experimental Methods

All animal procedures were approved by the Institutional Animal Care and Use Committee of the U.S. Army Institute of Surgical Research (Fort Sam, Houston, TX). Female pigs (35–45 kg) were anesthetized with initial injections of ketamine (1.0 ml each at 100 mg/ml) to effect followed by a continuous infusion at 1,000 mg/h, ventilated with positive pressure (adjusted to maintain arterial pCO_2 at 40 mmHg) and instrumented to record the physiological signals listed in Table 1. The chest was opened and the pericardium removed for the placement of flow probes around the aortic and pulmonary artery trunks. Catheters for measuring pressures were placed in the carotid artery, jugular vein, left ventricle and right ventricle. Pressure gauges were calibrated just before the experimental study and again at the end. The zero on the RV pressure gauge was adjusted so that baseline end-diastolic RV pressure was 2.5 mmHg (Altman and Dittmer 1971). All signals were collected at 500 Hz then reduced to 50 Hz resolution by sampling every tenth data point.

A wound to the heart wall was produced using a pneumatic device to propel a metal probe or fragment through the wall of either the left or right ventricle. No treatment of the wound was undertaken. Pigs that survived for two hours following the injury were classified as "survivors; " those dying earlier were "nonsurvivors." Survivors were euthanized immediately after the 2-h post-injury period. Among the experimental group there were seven survivors with complete data sets that were included in the present study. Seven randomly selected nonsurvivors that died at least 5 min after injury and that had complete data sets were used for comparing the surviving and nonsurviving groups.

Model Description

Development of the Closed-loop Circulatory Model

The model was simplified from the point of view of supplying blood to a distributed set of organs but was adequate to reproduce experimentally observed pressure waveforms in all parts of the circulation and flow waveforms in the aorta. The pulmonary circulation was treated as a single path with 3 arterial segments, capillaries, a shunt, and one venous segment emptying into the left atrium (LA). The LA and left ventricle (LV) were treated as bellows pumps with valves, described below, as were the right atrium (RA) and right ventricle (RV). The systemic circulation was composed of a single path with 4 arterial segments, capillaries and 2 venous segments. A branch from the aorta just downstream from the aortic valve represented the coronary circulation, consisting of epicardial arteries, intramyocardial arteries, capillaries, and a single venous segment emptying into the RA.

As in Windkessel models (Sagawa et al. 1990), the dynamics of compliant segments of the heart and systemic, pulmonary and coronary circulations were defined by a passive pressure–volume (PV) relationship, a resistance, and in the case of the great arteries, an inertance. Vascular PV relationships have been well characterized by Drzewiecki et al. (1997) as nearly linear at near the unstressed (zero-pressure) volume V_{rest} and gradually increasing in stiffness (becoming concave upward as compliance decreases) at higher pressures. The PV curve is concave downward at negative transmural pressures as the vessel collapses. Because no hypertensive situations were encountered or modeled, a linear approximation was used at $V > V_{rest}$ and a curvilinear description in the region of collapse below V_{rest}.

$$rlP_T = (V - V_{rest})/C - \Psi$$
$$\text{with } \Psi = K_{XP}/(e^{V/K_{XV}} - 1) \tag{1}$$

where P_T and V are the transmural pressure and volume, C is the compliance at volumes above the unstressed volume V_{rest}. Ψ dominates the PV curve at volumes below V_{rest} and is negligible above K_{XV} ml. K_{XP} and K_{XV} are curve-shaping constants. The curve is tangent to the pressure axis $V = 0$, that is, it goes toward $-\infty$ at small volumes. The compliance C' at $V' < V_{rest}$ was thus volume-dependent: $C'(V) = dV/dP$. See Eq. A.37 in the appendix. The values

of the curve-shaping constants in the coronary circulation (K_{XP1} and K_{XV1}) were smaller than for the other circulatory segments with larger unstressed volumes. The linear PV relationship at volumes above V_{rest} ignores the increase in elastance (decrease in compliance) that occurs in reality. A potential second term such as $a \times (V - V_{rest})^{\alpha}$ with $0.05 < a < 0.1$ and $2 \leq \alpha \leq 3$ was explored as an amendment to Eq. 1 but had negligble effect on solutions fitting the data in these studies since pressures were hypotensive.

In the experiments the chest and pericardium were open, so neither respiratory nor pericardial influences on the circulation were incorporated into the model. Transmural pressures were used in all PV calculations, and external pressure was assumed to be zero except in the intramural coronary vessels where the intramyocardial pressure P_{IM} was taken to be half the absolute left ventricle chamber pressure $PLV/2$, as in Eqs. A.82 and A.83 in the appendix. Gravitational effects were neglected.

Forward flows in vascular segments were calculated using the fluid analog of Ohm's law assuming constant resistance in each segment, independent of local pressure and volume:

$$F = \frac{\Delta P}{R} \qquad (2)$$

where F is forward flow, R is resistance, and ΔP is pressure drop across the segment, respectively. Radial flow due to compliance (flow that either increases or decreases segment volume) was the difference between segmental inflow (F_{inflow}) and outflow ($F_{outflow}$):

$$F_{radial} = \frac{dV}{dt} = F_{inflow} - F_{outflow} \qquad (3)$$

The Four-chambered Heart (Eqs. A1–A26)

The heart is composed of a pair of two-valved bellows pumps. Inflow is passive, but outflow is driven by the time-varying elastances of the chambers as used by Rideout (1991). The activation function of Heldt et al. (2002; see also Eqs. A.1–A.3) defines the shape of the time-varying elastance curves between the diastolic pressure elastance and a maximum elastance. The baroreceptor-dependent contractility multiplier af_{CON} increases the systolic elastance of the ventricles with arterial hypotension, and decreases it with hypertension.

Time-dependent unstressed volumes are used to relate transmural pressure and volume in all heart chambers: the elastance of the chamber is multiplied by the difference between the chamber's volume and its unstressed volume to give transmural pressure. As elastance increases during systole, the unstressed volume of the heart chamber decreases toward a minimum. Then, during diastole, elastance drops to its minimum and the unstressed volume rises to its maximum. This time-varying unstressed volume curve follows the shape of the Heldt et al. (2002) activation function's reflection about the x-axis. To avoid the generation of unrealistically large negative pressures in the ventricles during hypovolemia, the unstressed systolic ventricular volumes increase with lowered end-diastolic volumes Eq. A.16.

Systemic Circulation (Eqs. A27–A60)

The systemic circulation is comprised of seven vascular segments: proximal aorta, distal aorta, arteries, arterioles, capillaries, veins, and the vena cava. The arterioles, veins and vena cava have unique nonlinear PV relationships (Lu et al. 2001) that are described in Eqs. A.38–A.40, A.42, and A.43, respectively, and the PV relationships of the remaining segments follow Eq. 1. The resistances of the arterioles and vena cava (Eqs. A.59 and A.60) are also nonlinear and volume-dependent. Through the baroreceptor equations described subsequently, arteriolar resistance increases with lowered ABP, simulating the vasomotor compensatory feedback mechanism during hypotension. All other resistances throughout the systemic, pulmonary and coronary circulation are constant, independent of volume. Inertance elements are included in the proximal and distal aorta in order to simulate high-frequency features of the pressure waveforms in the great arteries caused by wave reflections at arterial bifurcations.

Pulmonary Circulation (Eqs. A61–A77)

The pulmonary circulatory segments include the proximal pulmonary artery, distal pulmonary artery, small arteries, capillaries and veins. All resistances are constant, and all PV relationships are of the form of Eq. 1. Inertance elements are included in the proximal and distal pulmonary artery segments to simulate wave-reflections.

Coronary Circulation (Eqs. A78–A93)

The seven coronary segments modeled by Zinemanas et al. (1994) were condensed into four segments for the closed-loop and open-loop models: epicardial arteries, intramyocardial arteries, coronary capillaries, and coronary veins. The intramyocardial arteries and capillaries are under the influence of the simulated intramyocardial pressure as described in Eq. 3. Therefore the transmural pressure in these segments is the difference between the chamber pressure and

the intramyocardial pressure, whereas elsewhere the chamber and transmural pressures are equal. All PV relationships in the coronary network are characterized using Eq. 1. Resistances were constant through the cardiac cycle.

Baroreceptors (Eqs. A94–A100)

The baroreceptor model of Wesseling et al. (1992) was implemented as by Lu et al. (2001). Aortic baroreceptor neural outflow to the brain was generated as a second-order response to the proportional and derivative aortic pressure signal. This in turn drives the level of signal in efferent pathways controlling maximum cardiac elastance and peripheral resistance. In our closed-loop and open-loop models, the baroreceptor feedback on heart rate was removed, and measured HR was used to initiate each beat.

Open-loop Models for Cardiac Output and Total Blood Volume Estimates

Our application strategy for estimating post-injury hemodynamics was to tune the closed-loop model described above to match the baseline hemodynamics of each experimental animal, then use the tuned parameters in conjunction with observed post-injury measurements to drive a similar *open-loop* model to estimate dynamics. The rate of hemorrhage during the experiments was not controlled and might have decreased or remained unabated over time, so we did not wish to rely on a *closed*-loop model parameterized with a specific injury (such as a resistive conduit for blood loss) for post-injury solutions. Instead, we used open-loop model forms driven by observable measurements obtained continuously. Neither hemorrhage rate nor wound location are required for model solutions using this method.

Two slightly different open-loop model variations were used for estimating CO and TBV (Fig. 1). The CO estimation model, detailed in an electrical analog schematic in Fig. 2, is "opened" immediately downstream of the proximal aorta segment and uses measured ABP and HR as inputs. The ABP waveform acts as the aortic afterload at the most downstream end of the circulatory loop, the proximal aorta, and is also used as the input to the baroreceptor system. At the most upstream end of the circulation, the distal aorta, a nonpulsatile aortic flow input function adjusts automatically to match the model-derived distal aortic pressure to the measured mean ABP (Eq. A.27). The model CO estimate is taken as the smoothed flow across the pulmonary valve (Eq. A.28), fulfilling the primary goal of providing an estimated CO to be compared with the CO measured via the flowmeters.
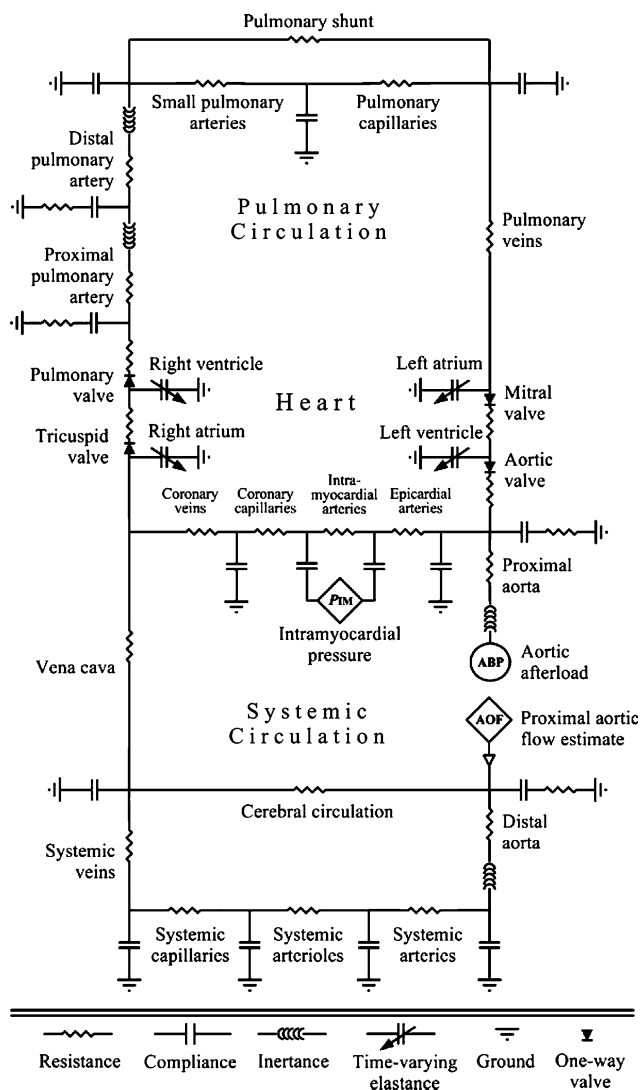

Fig. 2 Electrical analog schematic of the circulatory model used for cardiac output estimation. Symbols for components are at bottom

Secondarily, estimates of TBV, total blood volume, were obtained using a second open-loop model that was modified slightly from the CO estimation model. In addition to the ABP and HR inputs, *measured* CO is used as input flow to the circulatory system at the aortic valve. The double slashes through the baroreceptor outflow in Fig. 1 indicate that systemic arteriolar resistance is decoupled from the baroreceptor and is calculated from an estimate of *total* peripheral resistance and the sum of the remaining systemic segmental resistances:

$$R_{SA} = \frac{MAP_{MEAS} - EDP_{RV}}{CO_{MEAS}} - (R_{AOP} + R_{AOD} + R_{SAP} + R_{SC} + R_{SV} + R_{VC} + R_{RA}) \quad (4)$$

Here MAP_{MEAS} and CO_{MEAS} are the measured mean arterial blood pressure and cardiac output. The first term on

the right side thus gives TPR equal to the pressure drop across the entire peripheral circulation divided by measured CO, and EDP_{RV} is the model-estimated right ventricular end-diastolic pressure. The other terms in Eq. 4 are defined in Table 2. Noise-induced fluctuations in the arteriolar resistance R_{SA} at low CO, which can introduce numerical problems, were smoothed by limiting it to a maximum of 5 mmHg $\times$ s/ml (6,664 dyn $\times$ s/cm^5) to maintain stability.

TBV was calculated continuously by summing the volumes of all twenty circulatory segments. The CO estimation model can provide TBV estimates as well, since both open-loop systems contain the same circulatory structure. However, these estimates are affected by error in the estimated CO, whereas CO in the TBV estimation model is taken from measurement. The post-injury TBV estimated from both types of open-loop model analyses were each recorded for the time course of the study in order to allow comparison.

To prepare a version of the CO estimation model for public use, the model was hand-tuned to match human reference data; Table 2 lists the parameter values used for the resistances, compliances, unstressed volumes, and inertances throughout this model. Target reference values for model pressures, volumes and flows are also listed in this table, and the system was tuned so that corresponding variables were within 5% of these values in the steady state. Tables 3 and 4 list the other parameters and variables used in the hand-tuned reference human model, and Table 5 lists the initial conditions of the model's state variables. Values used for parameterizing the pig studies were not published in these tables because we felt that a compilation of reference human values for blood volumes, pressures and flows would be more useful to researchers. The hand-tuned, reference human CO estimation model is available online at http://www.nsr.bioeng.washington.edu/PLN/Members/mneal/COest/document_vie.

Methods of Analysis and Prediction

Parameterization to Subject-specific Baseline Hemodynamics

A computer program developed in the bash shell scripting language was used to optimize the parameters of the closed-loop HIP model and provide a simulation of each subject's pre-injury hemodynamics by fitting the model to measured blood pressures and flows. The optimized parameter values were then used in the open-loop modeling in order to estimate the post-injury timecourses of CO and TBV.

In order to tune resistances, compliances, inertances and other hemodynamic parameters in the closed-loop model,

the distribution of blood volumes, pressures, and flows in each subject had to be determined. Given that only seven continuous hemodynamic signals were recorded on each pig, "textbook" literature values were used to complete each subject's distribution of blood volumes, pressures and flows. Table 6 shows which physiological values used in the tuning procedure were measured and which were taken from the literature.

Once the entire set of target volumes, pressures and flows was determined for a particular subject, circulatory parameters were tuned so that model steady-state results would match these target values. The values for variables and parameters listed in Table 6 were used as starting values for each subject using methods outlined below. Parameters were optimized to fit model solutions to the pre-injury baseline data under JSim, a mathematical simulation environment available through the National Simulation Resource: http://www.physiome.org/jsim.ht.

To begin the parameterization of a particular subject's baseline model, the program read in the measured pulmonary artery flow (PAF), ABP, and LVP signals from a user-designated, 1-min segment of pre-injury data and recorded mean baseline values for CO, ABP_S, ABP_D, MAP and EDP_{LV}. In all experimental animals the baseline data used for parameterization was collected less than 2 min prior to injury.

Calculation of Initial Volumes

Baseline TBV was estimated for control conditions from pig weight using a formula from Altman and Dittmer (1971):

$$TBV\,(ml) = 65\,(ml/kg) \times W\,(kg) \qquad (5)$$

where W is the weight of the pig and TBV is the total amount of blood in circulation. The percentage of TBV in each circulatory segment (see Table 2 for values) was then set according to literature values obtained from various sources (Avolio 1980; International Commission on Radiological Protection 2003; Kassab et al. 1993; Kassab et al. 1994; Lu et al. 2001; Rosse and Rosse 1997; Toyota et al. 2002).

Compliances

In order to tune compliance parameters for each pig, the parameterization program computed the target transmural pressures in each segment throughout the circulation. Some of these pressures were calculated from subject data, others were estimations based solely on literature values (Altman and Dittmer 1971; Milnor 1982; Mohrman

Table 2 Values of circulatory model parameters and variables for the hand-tuned reference human CO estimation model

Circulatory segment ($_{SUBSCRIPT}$)	Resistance R_x (dyn*sec/cm^5)	Compliance C_x (ml/mmHg)	Unstressed volume $V_{x,0}$ (ml)	Inertance L_x (mmHg*sec^2/ml)	Pressure P_x (mmHg)	Volume V_x (ml)	Flow F_x (L/min)
Proximal aorta ($_{AOP}$)	0.13	0.26	9.5	1.0 E-5	94.2	34.3	6.24
Distal aorta ($_{AOD}$)	17.3	0.64	23.1	2.0 E-5	94.2	83.3	5.46
Systemic arteries ($_{SAP}$)	4.0	1.48	52.9		93.0	191	5.46
Systemic arterioles ($_{SA}$)	893, A.59	A.38–A.40	A.38–A.40		92.7	520	5.46
Systemic capillaries ($_{SC}$)	206	5.77	71.0		32.1	256	5.46
Systemic veins ($_{SV}$)	184	A.42	1,700		18.0	2,889	5.46
Vena cava ($_{VC}$)	40.0, A.60	A.43	130		5.4	240	6.24
Right atrium ($_{RA}$)	1.33	max: 11.76 min: 7.69	max: 60.0 min: 53.0		2.6	87.6	6.5
Right ventricle ($_{RV}$)	0.13	max: 29.14 min: 1.89	max: 103 min: 53.5		2.5 (EDP$_{RV}$)	176 (EDV$_{RV}$)	6.5
Proximal pulmonary artery ($_{PAP}$)	0.13	1.45	9.8	1.8 E-4	17.7	35.3	6.5
Distal pulmonary artery ($_{PAD}$)	40.0	2.53	17.2	1.9 E-4	17.7	61.8	6.5
Small pulmonary arteries ($_{PA}$)	75.3	3.1	17.2		14.4	61.8	6.37
Pulmonary shunt ($_{PS}$)	5,780				14.4	0	0.13
Pulmonary capillaries ($_{PC}$)	42.6	9.12	29.4		8.4	106	6.37
Pulmonary veins ($_{PV}$)	0.13	52.3	171		5.01	292	6.5
Left atrium ($_{LA}$)	1.33	max: 5.40 min: 3.33	max: 70.0 min: 40.0		5.0	87.6	6.5
Left ventricle ($_{LV}$)	0.13	max: 10.8 min: 0.19	max: 71.8 min: 23.7		5.0 (EDP$_{LV}$)	126 (EDV$_{LV}$)	6.5
Epicardial arteries ($_{COREPI}$)	7,040	0.074	2.7		94.2	9.7	0.26
Intramyocardial arteries ($_{CORINTRA}$)	13,500	0.13	2.7		71.3	9.7	0.26
Coronary capillaries ($_{CORCAP}$)	5640	0.94	2.5		27.3	9.1	0.26
Coronary veins ($_{CORVN}$)	1970	2.45	14.4		9.0	24.6	0.26
Cerebral circulation ($_{CRB}$)	9100				94.2	0	0.78
Heart rate: 77 beats/min							

Appendix equations, A.#, are referenced for segments with unique pressure–volume relationships and/or nonlinear resistances. Target steady-state averages (rounded) are given for chamber pressure, volume and flow variables. Target total blood volume is 5,300 ml. Model steady-state values are within 5% of target values

Table 3 Values of parameters used in the hand-tuned, reference human cardiac output estimation model not listed in Table 2

Parameter	Name	Definition	Value	Units
Parameters of pressure-volume relationships: Heart				
$E_{MAX,LA}$	Elastance	Maximum left atrial elastance	0.3	mmHg/ml
$E_{MAX,LV1}$	Elastance	Initial estimate of maximum left ventricle elastance	5.4	mmHg/ml
$E_{MAX,RA}$	Elastance	Maximum right atrial elastance	0.13	mmHg/ml
$E_{MAX,RV1}$	Elastance	Initial estimate of maximum right ventricle elastance	0.53	mmHg/ml
$E_{MIN,LA}$	Elastance	Minimum left atrial elastance	0.19	mmHg/ml
$E_{MIN,LV}$	Elastance	Minimum left ventricular elastance	0.093	mmHg/ml
$E_{MIN,RA}$	Elastance	Minimum right atrial elastance	0.085	mmHg/ml
$E_{MIN,RV}$	Elastance	Minimum right ventricular elastance	0.034	mmHg/ml
KE_{LV}		Scaling factor for maximum left ventricle elastance	1.0	
KE_{RV}		Scaling factor for maximum right ventricle elastance	1.0	
$Ts2$	Frequency	Unit balance scalar for Ts_a and Ts_v variables	1.0	Hz
V_{LAd0}	Volume	Left atrium unstressed end-diastolic volume	70	ml
V_{LAs0}	Volume	Left atrium unstressed peak-systolic volume	40	ml
V_{LVd0}	Volume	Left ventricle unstressed end-diastolic volume	72	ml
V_{LVs0}	Volume	Left ventricle unstressed peak-systolic volume	23	ml
V_{RAd0}	Volume	Right atrium unstressed end-diastolic volume	60	ml
V_{RAs0}	Volume	Right atrium unstressed peak-systolic volume	53	ml
V_{RVd0}	Volume	Right ventricle unstressed end-diastolic volume	103	ml
V_{RVs0}	Volume	Right ventricle unstressed peak-systolic volume	53	ml
Parameters of pressure-volume relationships: Systemic circulation				
$D2$	Pressure	Offset for vena cava PV relationship	−5	mmHg
D_0	Volume	Active vasomotor tone volume parameter for systemic arterial pressure	50	ml
$K1$	Elastance	Scaling factor for vena cava PV relationship	0.046	mmHg ml^{-1}
$K2$	Pressure	Scaling factor for vena cava PV relationship	0.374	mmHg
K_C	Pressure	Active vasomotor tone scaling parameter for systemic arterioles	498	mmHg
$K_{CO,MAP}$		Gain for automatically-adjusting aortic flow estimate	3	l/(mmHg· min^2)
K_{SV}		Optimized scaling factor for systemic venous PV relationship	0.74	
K_{V1}		Initial estimate of scaling factor for baseline sytemic venous PV relationship	30.2	
$Kp1$	Pressure	Passive vasomotor tone scaling parameter for systemic arteriolar pressure	0.03	mmHg
$Kp2$	Pressure	Passive vasomotor tone scaling parameter for systemic arteriolar pressure	0.05	mmHg
K_{XP}	Pressure	Low volume PV curve shaping constant	2	mmHg
K_{XP1}	Pressure	Low volume PV curve shaping constant for coronaries	1	mmHg
K_{XV}	Volume	Low volume PV curve shaping constant	8	ml
K_{XV1}	Volume	Low volume PV curve shaping constant for coronaries	1	ml
τ_P		Passive vasomotor tone constant for systemic arterial pressure	0.1	ml^{-1}
V_0	Volume	Vena cava unstressed volume	130	ml
$V_{MAX,SV}$	Volume	Maximum volume of systemic veins	3,380	ml
$V_{MAX,VC}$	Volume	Maximum volume of vena cava	351	ml
$V_{MIN,VC}$	Volume	Minimum volume of vena cava	50	ml
$V_{SA,0}$	Volume	Minimum volume of systemic arterioles	486	ml
Visco-elastic (radial flow) resistances				
R_{SA0}	Resistance	Offset for systemic arteriolar resistance	774	dyn s/cm^5
R_{TPAD}	Resistance	Distal pulmonary artery radial flow resistance	267	dyn s/cm^5
R_{TPAP}	Resistance	Pulmonary artery trunk radial flow resistance	133	dyn s/cm^5
R_{TAOD}	Resistance	Radial flow resistance of distal aorta	1330	dyn s/cm^5
R_{TAOP}	Resistance	Radial flow resistance of proximal aorta	26.7	dyn s/cm^5

Table 3 continued

Parameter	Name	Definition	Value	Units
Parameters of variable resistances				
Kr	Resistance	Systemic arteriolar resistance scaling constant	13.3	dyn s/cm^5
KR	Resistance	Scaling factor for vena cava resistance	1.33	dyn s/cm^5
R_0	Resistance	Vena cava resistance offset parameter	33.3	dyn· s/cm^5
$V_{SA,MAX}$	Volume	Maximum volume of systemic arterioles	578	ml
Time constants for filtering measured data				
$\tau_{ABP,FOL}$	Time	Time constant for arterial pressure derivative	0.001	s
τ_{CO}	Time	Time constant for cardiac output estimate	15	s
$\tau_{CO,MAP}$	Time	Time constant for aortic flow estimate	20	s
τ_{MAP}	Time	Time constant for measured mean arterial pressure	2	s
Parameters for discrete heart functions				
EDV_{LV}	Volume	Baseline end-diastolic volume of left ventricle	126	ml
EDV_{RV}	Volume	Baseline end-diastolic volume of right ventricle	176	ml
offv	Time	Offset for matching diastolic/systolic timing of measured arterial blood pressure curve	0.026	s
PR_{INT}	Time	P wave to R wave interval	0.12	s
Ts_aK	Time	Scaling factor to set systolic fraction of atrial contraction cycle	0.35	s
Ts_vK	Time	Scaling factor to set systolic fraction of ventricular contraction cycle	0.2	s
Baroreceptor parameters				
a	Time	Time constant for baroreceptor firing rate	0.001	s
a_{CON}		Normalized frequency offset for ventricular contractility	0.3	
a_{MIN}		Contractility control offset	−2.81	
a_{VASO}		Normalized frequency offset for systemic arteriolar resistance	−0.47	
$a1$	Time	Time constant for baroreceptor firing rate	0.036	s
$a2$	Time	Time constant for baroreceptor firing rate	0.0018	s
b_{CON}		Time constant for efferent sympathetic contractility firing	0.7	
b_{MIN}		Contractility control offset	0.7	
K		Baroreceptor gain	0.99	s^{-1} mmHg^{-1}
K_{CON}		CNS gain for contractility control	1	1
K_{VASO}		CNS gain for vasomotor tone control	1	1
Ka		Contractility control scaling factor	5	
Kb		Contractility control scaling factor	0.5	
l_{CON}	Time	CNS time delay for contractility control	3	s
l_{VASO}	Time	CNS time delay for vasomotor tone control	3	s
$N_{0,CON}$	Frequency	Frequency parameter for efferent sympathetic contractility firing	110	s^{-1}
$N_{0,VASO}$	Frequency	Frequency parameter for efferent sympathetic heart rate firing	110	s^{-1}
τ_{CON}	Time	Time parameter for efferent sympathetic contractility firing	0.04	s
τ_{VASO}	Time	Time parameter for efferent vasomotor tone firing	0.04	s
T_{CON}	Time	CNS time parameter for contractility control	10	s
T_{VASO}	Time	CNS time parameter for vasomotor tone control	6	s

and Heller 2003; Scher 1989; Zinemanas et al. 1994). For circulatory segments with undefined rest volumes, compliances were calculated by setting V_{rest} and Ψ (see Eq. 1) to zero and then dividing the mean normal segment volume by its mean normal transmural pressure. The remaining nonlinear PV relationships in the distal systemic arteriolar, systemic venous and vena cava segments were tuned by adjusting the parameters K_{SV}, K_1, and K_C, respectively.

Except for the intramyocardial arteries and capillaries, which are under the influence of intramyocardial pressure, the transmural pressures throughout the circulation used for hand-tuning the reference human model were the same as the distribution of chamber pressures found in Table 2.

Table 4 Variables of the hand-tuned, reference human cardiac output estimation model not listed in Table 2

Variable	Name	Definition	Units
Four-chambered heart			
E_{LA}	Elastance	Time-varying elastance of left atrium	mmHg/ml
E_{LV}	Elastance	Time-varying elastance of left ventricle	mmHg/ml
$E_{MAX,LV}$	Elastance	Maximum left ventricular elastance	mmHg/ml
$E_{MAX,RV}$	Elastance	Maximum right ventricular elastance	mmHg/ml
E_{RA}	Elastance	Time-varying elastance of right atrium	mmHg/ml
E_{RV}	Elastance	Time-varying elastance of right ventricle	mmHg/ml
HP	Time	Heart period from measured ECG	s
HR	Frequency	Heart rate	min^{-1}
HR_a	Frequency	Discrete heart rate used for atrial activation function	Hz
HR_v	Frequency	Discrete heart rate used for ventricular activation function	Hz
m		Indexed heartbeat used for ventricular activation function	
n		Indexed heartbeat used for atrial activation function	
$t_{a,REL}$	Time	Time from start of last atrial contraction	s
t_{HB}	Time	*R* wave start time (from ECG) indexed by heartbeat number	s
t_{PWAVE}	Time	Start of contraction in atrial activation function	s
t_{RWAVE}	Time	Start of contraction in ventricular activation function	s
$t_{v,REL}$	Time	Time from start of last ventricular contraction	s
Ts_a	Time	Discrete systolic interval for atria	s
Ts_v	Time	Discrete systolic interval for ventricles	s
V_{LA0}	Volume	Unstressed volume of left atrium	ml
V_{RA0}	Volume	Unstressed volume of right atrium	ml
$Vvar_{LVs0}$	Volume	Left ventricle systolic unstressed volume	s
$Vvar_{RVs0}$	Volume	Right ventricle systolic unstressed volume	s
y_a		Atrial activation function	
y_v		Ventricular activation function	
Circulation			
ABP_{FOL}	Pressure	Time-shifted measured arterial blood pressure follower	mmHg
ABP_{MEAS}	Pressure	Measured arterial blood pressure	mmHg
ABP_{SHIFT}	Pressure	Time-shifted measured arterial blood pressure	mmHg
AOF_{MOD}	Flow	Aortic flow estimate	l/min
CO_{MOD}	Flow	Cardiac output estimate	l/min
$F_{RV,SM}$	Flow	Smoothed flow across pulmonary valve	l/min
K_V	Pressure	Scalar for systemic veins pressure-volume relationship	mmHg
MAP_{MEAS}	Pressure	Measured mean arterial blood pressure	mmHg
MAP_{MOD}	Pressure	Simulated mean arterial blood pressure	mmHg
$P_{CORCAP,C}$	Pressure	Coronary capillary chamber pressure	mmHg
$P_{CORINTRA,C}$	Pressure	Intramyocardial arteries chamber pressure	mmHg
$P_{COREPI,C}$	Pressure	Epicardial arteries chamber pressure	mmHg
$P_{CORVN,C}$	Pressure	Coronary veins chamber pressure	mmHg
P_{IM}	Pressure	Intramyocardial pressure	mmHg
$P_{SA,A}$	Pressure	Active systemic arteriolar pressure component	mmHg
$P_{SA,P}$	Pressure	Passive systemic arteriolar pressure component	mmHg
SV	Volume	Stroke volume	ml
TBV	Volume	Total blood volume	ml
$V_{CORCIRC}$	Volume	Volume of blood in coronary circulation	ml
V_{HEART}	Volume	Volume of blood in heart	ml
V_{PULART}	Volume	Volume of blood in pulmonary arterial system	ml

Table 4 continued

Variable	Name	Definition	Units
V_{SYSART}	Volume	Volume of blood in systemic arterial system	ml
V_{SYSVEN}	Volume	Volume of blood in systemic venous system	ml
Baroreceptor			
af_{CON}		Continuous ventricular contractility scaling function	
af_{CON2}		Discrete ventricular contractility scaling function	
b_{VASO}		Scalar for normalization of efferent vasomotor control	
f_{CON}		Normalized firing rate for contractility control	
f_{VASO}		Normalized firing rate for vasomotor control	
N_{CON}	Frequency	Sympathetic firing rate at CNS for contractility control	Hz
N_{VASO}	Frequency	Sympathetic firing rate at CNS for vasomotor control	Hz
Nbr	Frequency	Firing frequency of baroreceptor	Hz
Nbr_t		Time derivative of baroreceptor firing frequency	Hz^2

Volume Constants in the Systemic Circulation

Published values of maximum, minimum and unstressed volume parameters throughout the systemic circulation (Lu et al. 2001) were all scaled by multiplying them by the ratio of the subject's total blood volume to a reference human blood volume: 5,300 ml (International Commission on Radiological Protection 2003). The parameters $V_{SA,0}$, $V_{MAX,VC}$, $V_{MIN,VC}$, V_0, $V_{SA,MAX}$ and $V_{MAX,SV}$ were tuned in this manner, and Appendix Eqs. A.39, A.60, A.43, A.59, and A.42 describe their use in the circulatory model.

Unstressed Heart Chamber Volumes

A formula from Klotz et al. (2006) based on data obtained from excised human, canine, and rat hearts was used to calculate unstressed diastolic ventricular volumes for the reference human model (1.36% of TBV for left ventricle, 1.94% of TBV for right ventricle). These same percentages were used for the pig unstressed diastolic volumes (Table 3). Peak systolic unstressed ventricular volumes were then estimated by multiplying the unstressed end-diastolic volumes by the ratio of the ventricle's end-systolic volume to end-diastolic volume. Unstressed atrial volumes that provided appropriate volumes and pressures in a prototype pig model created prior to the study were used in the parameterization program.

Ventricular Elastances

To calculate ventricular elastance values, estimates for baseline left and right ventricle end-diastolic volumes (EDV_{LV} and EDV_{RV}) were calculated by dividing the

subject's stroke volume by each ventricle's "textbook" ejection fraction (Table 6; see also Scher 1989, Marino 1998). Baseline left and right end-diastolic ventricular pressures (EDP_{LV} and EDP_{RV}), divided by their estimated end-diastolic pressure-generating volumes ($EDV_{LV} - V_{LVd0}$ and $EDV_{RV} - V_{LVd0}$), provided values for the ventricular diastolic elastance parameters $E_{MIN,LV}$ and $E_{MIN,RV}$. Initial computation of the maximum ventricular elastance parameters $E_{MAX,LV}$ and $E_{MAX,RV}$ was performed by dividing the baseline peak systolic ventricular pressures by the end-systolic pressure-generating volumes ($ESV_{LV} - V_{LVs0}$ and $ESV_{RV} - V_{LVs0}$). $E_{MAX,LV}$ and $E_{MAX,RV}$ were then multiplied by corresponding contractility parameters KE_{LV} and KE_{RV} that were optimized later in the parameterization process to determine the maximum elastance for each ventricle (see *Optimization*, below).

Resistances

Although a measure of pre-injury CO was available for all pigs, the baseline distribution of forward blood flow throughout the circulation had to be based on literature values. Each pre-injury, closed-loop model was tuned so that 12% of the total systemic CO flowed to the cerebral circulation (International Commission on Radiological Protection 2003), and 4% to the coronaries (Feigl 1989). In passage through the lungs, 2% of pulmonary artery flow was considered to be unaerated, a pulmonary shunt (Lu et al. 2001). The distribution of blood pressures and flows throughout the circulation was used to calculate resistances for the cerebral, systemic capillary, systemic venous, all pulmonary arterial, pulmonary capillary, pulmonary shunt, and coronary segments by dividing the pressure drop across the segment by the segment's forward flow (Eq. 2). Initial

Table 5 Initial conditions of state variables in the hand-tuned, reference human cardiac output estimation model

Variable	Initial condition	Units
Four-chambered heart		
V_{LA}	61.0	ml
V_{LV}	127	ml
V_{RA}	77.2	ml
V_{RV}	177	ml
Circulation		
AOF_{MOD}	6.25	l/min
F_{AOP}	−0.27	l/min
F_{AOD}	5.47	l/min
F_{PAD}	2.38	l/min
F_{PAP}	1.22	l/min
$F_{RV,SM}$	6.43	l/min
P_{AOP}	82.9	ml
V_{AOP}	30.2	ml
V_{AOD}	83.4	ml
$V_{CORINTRA}$	9.92	ml
V_{CORCAP}	10.1	ml
V_{CORVN}	23.9	ml
V_{PAD}	59.8	ml
V_{PAP}	30.4	ml
V_{PA}	51.5	ml
V_{PC}	105	ml
V_{PV}	308	ml
V_{SAP}	191	ml
V_{SA}	522	ml
V_{SC}	256	ml
V_{SV}	2940	ml
V_{VC}	244	ml
Baroreceptor		
N_{CON}	93.3	Hz
N_{VASO}	93.2	Hz
Nbr	82.2	Hz
Nbr_t	0.0013	Hz^2

See Tables 2 and 4 for variable definitions

values for the resistances of the proximal aorta and distal aorta were calculated using Poiseuille's Law and arterial geometry from Avolio (1980). Resistances of heart valves, pulmonary veins and systemic arteries were small and therefore had little influence, but for consistency were taken from the reference human model (see Table 2) and were used for all subjects in the study.

Systemic arteriolar resistance, R_{SA}, is not constant, but depends on baroreceptor influence. Therefore, when tuning the model, each parameter and variable in the R_{SA} Eq. A.59 must be set so that the efferent firing generated from the baseline blood pressure input to the baroreceptor results in the desired systemic arteriolar resistance. The initial

estimate of this resistance was computed using Eq. 2, given the putative pressure drop and forward flow across the arteriolar segment. However, this resistance was optimized later as described in the *Optimization* section below.

The vena cava has a nonlinear, volume-dependent resistance (Eq. A.60). The parameter $V_{MAX,VC}$ in this equation was adjusted proportionally to the subject's total blood volume as mentioned above. For the remaining parameters in the volume-resistance relationship of this segment (see Table 3) we used published values (Lu et al. 2001).

Inertances

The four inertance parameters for the great arteries, L_{AOP}, L_{AOD}, L_{PAP}, and L_{PAD}, were tuned initially using a formula based on the application of Newton's second law to a continuum in momentum:

$$L = \frac{\rho \times l^2}{V} \tag{6}$$

Here L, ρ, l, and V are inertance, blood density, segment length, and segment blood volume, respectively. Although initially set with formula-based values, the proximal and distal aortic inertance parameters were optimized later in the autoparameterization program to match the recorded baseline ABP curve. Pulmonary artery trunk and proximal pulmonary artery inertances were computed from Eq. 6 and held constant.

Optimization to Parameterize the Baseline Pre-injury Data

After the initial parameter set was calculated, further tuning to fit model solutions to the pre-injury data was undertaken using the Simplex optimizer (Nelder and Mead 1965) one of those available in the JSim simulation system. An initial optimization was performed to match model results to the target baseline values of EDV_{RV}, EDV_{LV}, CO and diastolic arterial blood pressure (ABP_D) by adjusting the ventricular elastance multipliers (KE_{LV} and KE_{RV}), the venous elastance multiplier (K_{SV}), pulmonary arterial resistance (R_{PA}), and systemic arteriolar resistance (R_{SA}). Generally speaking, this procedure set the balance between venous filling and the contractile emptying of the heart. The baroreceptor-dependent contractility multiplier (af_{CON}) was held constant at its target steady-state value of 1.0 during this optimization so it did not influence the tuning of the ventricular elastance parameters KE_{LV} and KE_{RV} (see Eqs. A.19 and A.22).

In order to match ABP_D, systemic arteriolar resistance (R_{SA}) was included in the optimization procedure. The

Table 6 Measured and "textbook" physiological values used to parameterize the subject-specific pig models for the pre-injury steady-state

Measured values (average ± SD)

Weight: 40.8 ± 2.4 kg

HR: 96.9 ± 17.2 beats/min

CO: 4.76 ± 0.94 l/min

ABP_S: 107.8 ± 17.4 mmHg

ABP_D: 68.7 ± 17.4 mmHg

MAP: 84.4 ± 17.5 mmHg

Peak LVP: 121.2 ± 21.2 mmHg

Peak RVP: 33.5 ± 5.6 mmHg

EDP_{LV}: 8.15 ± 3.08 mmHg

"Textbook" values

EDP_{RV}: 2.5 mmHg

Left ventricle ejection fraction: 67%

Right ventricle ejection fraction: 48%

Coronary flow to CO ratio: 0.04

Cerebral flow to CO ratio: 0.12

Pulmonary shunt flow to CO ratio: 0.02

Upstream systemic venous pressure: 18 mmHg

Upstream systemic capillary pressure: 32 mmHg

Blood density: 1.05 g/ml

Length of proximal pulmonary artery: 2.85 cm

Length of distal pulmonary artery: 3.90 cm

Left ventricle unstressed diastolic volume: 1.36% of TBV (36.1 ml for average TBV)

Left ventricle unstressed systolic volume: 0.43% of TBV (11.4 ml for average TBV)

Right ventricle unstressed diastolic volume: 1.94% of TBV (50.9 ml for average TBV)

Right ventricle unstressed systolic volume: 1.0% of TBV (26.5 ml for average TBV)

Distribution of total blood among the individual circulatory segments (see Table 2)

ABP_D: diastolic arterial blood pressure; ABP_S: systolic arterial blood pressure; CO: cardiac output; EDP_{LV}: end-diastolic left ventricle pressure; EDP_{RV}: end-diastolic right ventricle pressure; HR: heart rate; LVP: left ventricle pressure; RVP: right ventricle pressure; MAP: mean arterial blood pressure

initial estimate R_{SA} was computed using Eq. 2, but it is variable, depending on baroreceptor feedback, and, when tuning the closed-loop model, parameters in the R_{SA} Eq. A.59 must be adjusted so that the efferent firing rate generated from the baseline blood pressure input to the baroreceptor results in the desired systemic arteriolar resistance. First we optimized to find an improved value for R_{SA} when baroreceptor responses were decoupled. Then, using this value of R_{SA} as a start, a second, independent optimization process (described below) tuned baroreceptor parameters so that the final, fully integrated closed-loop model produced this target value for R_{SA} in the steady state.

The next optimization routine adjusted the baroreceptor gain parameter K so that the average baroreceptor firing frequency (Nbr) was set to a physiologically normal value of 95 impulses/s (Spickler et al.1967) given the measured ABP as input. A subsequent optimization routine adjusted the offset parameters a_{VASO} and a_{MIN} so that the normalized efferent vasomotor tone firing frequency (f_{VASO}, Eq. A.98) and heart contractility multiplier (af_{CON}) were set to their assumed baseline values of 0.5 and 1.0, respectively.

Given the other parameters in the equation for systemic arteriolar resistance (Eq. A.59) and the target steady-state values for f_{VASO} and V_{SA}, we calculated the value of an offset parameter R_{SA0} so that R_{SA} would match the target R_{SA} value computed during the first optimization described above.

These new values for baroreceptor-related parameters, along with the first set of optimized circulatory parameters, were copied and passed to a third optimization routine configured to match the model and measured ABP. Several parameters were adjusted simultaneously for this final optimization: forward flow resistance in the proximal and distal aorta (R_{AOP} and R_{AOD}), radial flow resistance in the distal aorta (R_{TAOD}), proximal and distal aortic inertances (L_{AOP} and L_{AOD}), proximal and distal aortic compliances (C_{AOP} and C_{AOD}), maximum left ventricular elastance (KE_{LV}) and the systemic venous elastance multiplier (K_{SV}). This optimization routine was interrupted three times after 200 iterations to adjust a time-shift parameter (*offv*) that aligned end-diastole of the recorded ABP signal with end-diastole of the corresponding model curve. Although resulting in subtle changes, these interruptions ensured that

the optimizer only matched diastolic portions of the model curve with diastolic portions of the empirical curve and likewise for systolic portions.

Optimizing the parameters involved in shaping the model ABP curve can take many hours to complete because of the large numbers of parameters and the many iterations required for convergence. The results showed good fits to measured ABP_D, ABP_S and MAP relatively early in the procedure, whereas fitting the more subtle within-beat cyclic contours of the measured ABP waveform took more time to optimize. Therefore, parameter values obtained after 1,100 iterations of this optimization were used.

In all, 74 parameters were adjusted to create each of the subject-specific parameter sets. Although many parameters were tuned, this process was constrained by the set of baseline experimental measurements and the assumed "textbook" values presented in Table 6. The average time to complete parameterization for a subject was 24 ± 7 (SD) hours on a 2.4 GHz processor.

After the automatic parameterization program finished, the optimized parameter set representing the baseline, pre-injury state of the subject was used in the open-loop circulatory models for estimation of CO and TBV from post-injury data. No parameter adjustments were made on post-injury data.

Numerical solutions to the equations were obtained at a time step of 0.02 s using the adaptive step solver CVODE (Cohen and Hindmarsh 1996) under JSim. Optimizations minimized ordinate-based least squares objective functions.

Statistical Analysis

Percent differences between target baseline measurements and corresponding model results were tabulated following the automated parameterization process. Assessment of error in model estimation of CO post-injury was based on root mean square (RMS) error, Bland-Altman (1986) and Pearson product correlation analyses. Bland-Altman analysis provides an assessment of parity between two measurement techniques by comparing the difference between two measurements against their average, and the Pearson correlation analysis measures the linear relationship between two data sets. The summation of all 20 circulatory segment volumes in the open-loop TBV estimation model provided post-injury blood loss estimates, and t-tests were performed to detect significant differences in blood loss between pigs that survived the two hour post-injury period and those that died. Paired t-tests were also used to detect differences between the TBV estimates of the two different open-loop models. $P < 0.05$ was considered significant in all cases.

Table 7 Average measured baseline values and differences between baseline model and measured values for all subjects

Measurement	Baseline values, $n = 14$ (average $\pm$ SD)	Percent difference between model and measured baseline values (average $\pm$ SD)
CO	4.76 ± 0.94 l/min	$1.8 \pm 0.6\%$
ABP_S	107.8 ± 17.4 mmHg	$0.6 \pm 0.4\%$
ABP_D	68.7 ± 17.4 mmHg	$1.5 \pm 1.3\%$
MAP	84.4 ± 17.5 mmHg	$1.6 \pm 1.0\%$
EDP_{LV}	8.2 ± 3.1 mmHg	$1.2 \pm 0.7\%$

CO: Cardiac output; ABP_S: systolic arterial blood pressure; ABP_D: diastolic arterial blood pressure; MAP: mean arterial blood pressure; EDP_{LV}: end-diastolic left ventricle pressure

Results

Matches to Baseline Hemodynamics

The average percent differences between the closed-loop, steady-state results for CO, ABP_S, ABP_D, MAP, and EDP_{LV} and their corresponding baseline physiological measurements are presented in Table 7. The average percent difference between all model results compared to measurement was $1.4 \pm 1.3\%$ SD for the 14 pigs, and survivors and nonsurvivors were fit equally well.

Cardiac Output Estimation

The model-estimated and measured CO for post-injury timecourses of two subjects, P132 and P168, are plotted in Fig. 3. These two animals gave the lowest and highest RMS scores among the 14 pigs. Figure 3A shows the timecourses of model variable values of CO together with the experimental flowmeter measures of CO. For study P132 the estimated and observed curves are close, but for P168 the difference is much greater, indicating that the model did not accurately represent the adaptability of the animal in this, the worst case. Figure 3B shows plots of the estimated CO versus measured CO and the R^2 correlation statistic for these two animals. Figure 3C shows Bland-Altman plots of the difference between measured and estimated CO pairs vs. their average, and dashed lines indicate biases and limits of agreement. The fits of estimated versus measured CO in P168 shows high RMS error, poor R^2 and large Bland Altman bias compared to these same measures of fit gathered from all 14 experiments in Table 8.

Post-injury CO_{MOD} and CO_{MEAS} data from each experimental animal were downsampled to 700 pairs per pig, and then concatenated into one combined dataset. A Bland-Altman plot of the difference between these CO_{MOD} and CO_{MEAS} values versus their average is

Fig. 3 Comparisons between model-estimated and measured cardiac output (CO) for the best fitted subject P132 and the worst, P168. (**A**) Model (line) and measured (circles) cardiac output versus time. Root mean square (RMS) error values are indicated. (**B**) Model versus measured cardiac output. Arrows indicate temporal direction. R^2 is the square of the correlation coefficient. (**C**) Bland-Altman plots. CO difference = (model cardiac output − measured cardiac output) versus CO average = (model cardiac output + measured cardiac output)/2. Biases (average CO difference) and limits of agreement are indicated
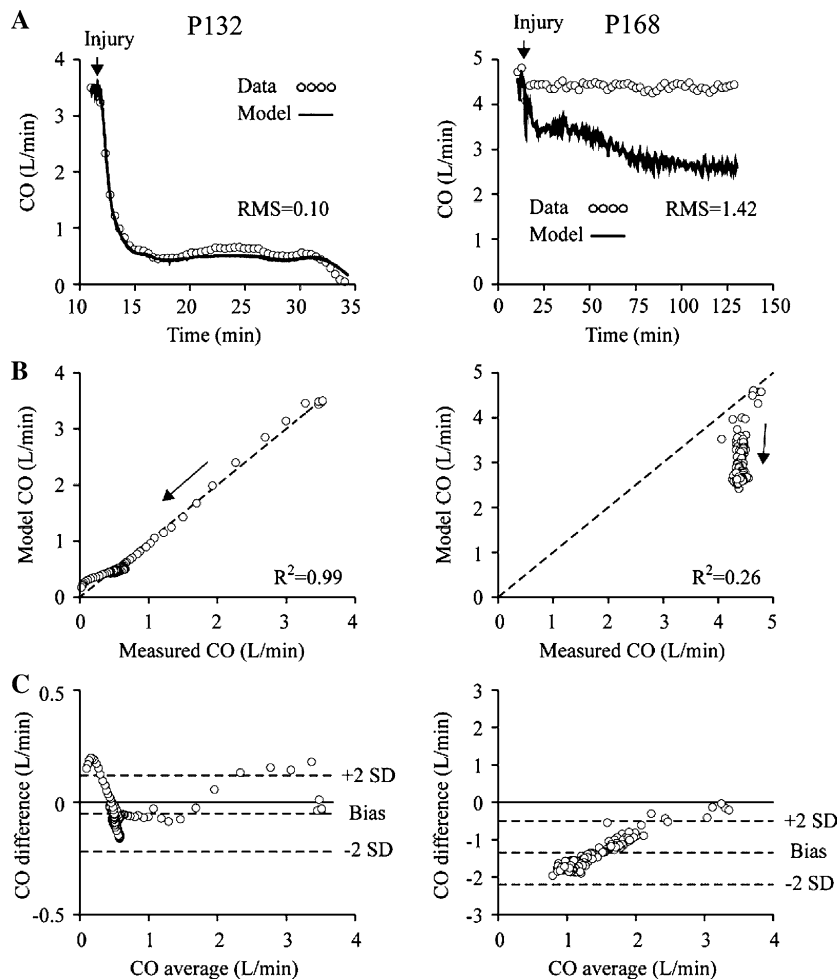
presented in Fig. 4. The bias and limits of agreement noted on the graph summarize the accuracy of the CO estimation method for the entire study group: *Bias* = −0.30 l/min, lower limit of agreement = −1.40 l/min, upper limit of agreement = 0.80 l/min. Fourteen percent of all CO estimates were accurate to within 0.1 l/min, 70% were within 0.5 l/min, 86% were within 1 l/min, and 100% were within 2 l/min.

Total Blood Volume Estimation

The CO estimation model and the TBV estimation model both provided estimates of TBV post-injury. The CO estimation model takes the estimated CO as valid and extrapolates further to estimate TBV, whereas the TBV estimation model uses the measured CO as input to the circulation. Maximum blood losses for each subject following hemorrhage, as a percentage of their initial TBV, are presented in Fig. 5 along with the subject's time to death. Figure 5A shows the blood loss results from the CO

estimation model, and Fig. 5B shows the results from the TBV estimation model. Using the CO estimation model, nonsurvivors lost an average of 53% of their baseline TBV and survivors lost 21%. Using the TBV estimation model, nonsurvivors lost an average of 50% of their baseline TBV and survivors lost only 17%. The difference in estimated blood loss between survivors and nonsurvivors was significant using results from either model (*t*-tests, $P < 0.0001$ for both). The difference between the results of the two models was significant only among the surviving population (paired *t*-test, $P < 0.05$), but not among nonsurvivors (paired *t*-test, $P = 0.54$), nor for the combined group of all experimental subjects (paired *t*-test, $P = 0.098$).

Discussion and Conclusions

The model presented here is reduced from a more complete model available on our website at http://www.physiome. org/redirect/HIHwIindex.html (not yet published with peer review). In addition to the circulatory and baroreceptor

Table 8 Cardiac output estimation: measurements of fit between the estimated and measured post-injury cardiac output for all animals in the study

Subject ID	Time to death (min)	RMS error (L/min)	R^2	Bland-Altman bias (L/min)
P78	120+	0.36	0.42	−0.30
P79	106	1.08	0.54	−0.99
P80	5	0.33	0.98	0.26
P87	120+	0.43	0.55	−0.35
P107	87	0.61	0.86	−0.56
P127	120+	0.90	0.13	−0.85
P132	23	0.10	0.99	−0.05
P138	120+	0.38	0.78	−0.37
P143	120+	0.43	0.74	−0.42
P168	120+	1.42	0.26	−1.35
P179	5	0.37	0.98	0.24
P189	120+	0.18	0.57	0.07
P193	8	0.31	0.98	0.28
P198	21	0.30	0.95	0.21
Average ± SD		0.51 ± 0.37	0.69 ± 0.29	−0.30 ± 0.51

RMS: root mean square; R^2: square of the correlation coefficient. A time to death of 120 + min indicates survival through the post-injury observation period
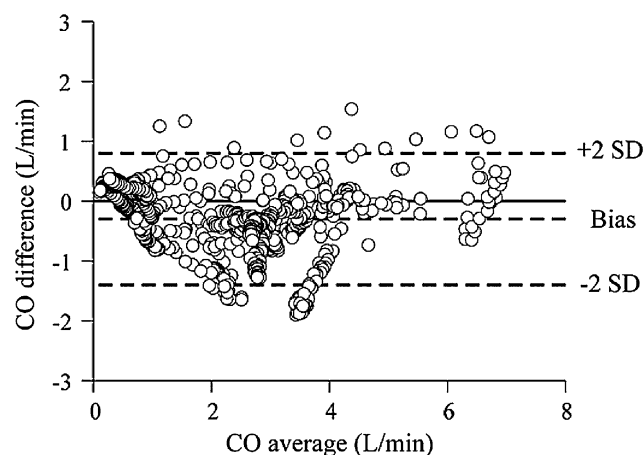
Fig. 4 Cardiac output estimation: Bland-Altman plot for the combined cardiac output estimation results of all 14 study animals. Bias and upper and lower limits of agreement are −0.30, 0.80 and −1.40 l/min, respectively. CO difference = (model cardiac output − measured cardiac output), CO average = (model cardiac output + measured cardiac output)/2

components detailed here, this parent model also contains a pericardium (Sun et al. 1997), baroreceptor influence on heart rate (Lu et al. 2001), carotid chemoreceptor influence on respiratory minute volume (Lu et al. 2002), airway mechanics and ventilation (Athanasiades et al. 2000),
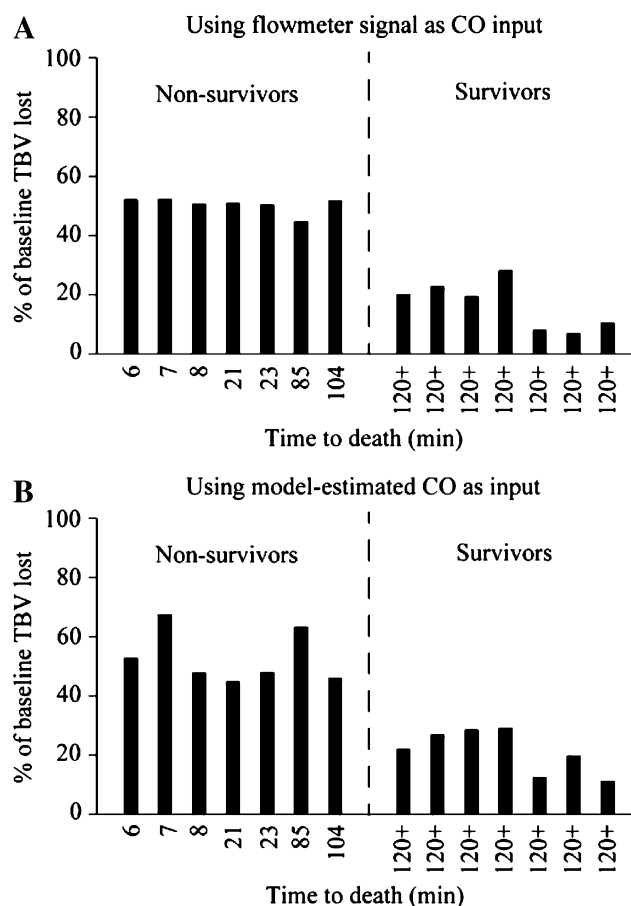
Fig. 5 Model-estimated percent total blood volume loss following hemorrhage vs. time to death. (**A**) Cardiac output estimation model: percent total blood volume lost. Survivors had significantly lower model-predicted blood loss than nonsurvivors (*t*-test, P < 0.0001). (**B**) Total blood volume estimation model: percent total blood volume lost. Survivors had significantly lower model-predicted blood loss than nonsurvivors (*t*-test, P < 0.0001)

alveolar gas exchange (Lu et al. 2002), and blood gas handling of oxygen, carbon dioxide, bicarbonate and pH (Dash and Bassingthwaighte 2004, Dash and Bassingthwaighte 2006). While in theory the parent model should be better at estimating CO and blood volume than our reduced form, this has not been tested and seems somewhat unlikely given the models are nearly identical in their circulatory structure. Both the fuller and reduced models can be expected to fail at the end of a long period of whole-body underperfusion since there is no accounting for shock responses or effects on vascular or cardiac contractility. The reduced model form was chosen for the testing of its ability to provide surrogate measurements since it can be run in real time, and therefore in principal would be applicable to data monitoring and analysis during emergency care scenarios.

Advancements and Differences from Earlier Models

The systemic and pulmonary circulatory model presented here differs modestly but significantly from preceding models (Lu et al. 2001; Rideout 1991; Zinemanas et al. 1994) as follows: (1) sympathetic vasoconstriction from baroreceptor feedback is localized at the fourth level of the arterial system in the arteriolar segment [further downstream than the location used by Lu et al. (2001) and Rideout (1991)] to more faithfully represent the general architecture of the arterial system; (2) a low-resistance arterial segment (subscript SAP, systemic arteries proximal) is placed between the distal aorta and arteriolar segments to represent large conductive arteries; (3) the cerebral circulatory segment, which is taken to be a zero-volume vessel, flows between the distal aortic and vena cava nodes; and (4) pulmonary capillary resistance is constant (that is, independent of alveolar volume) since mechanical influences of the airways were not modeled.

Intramyocardial arteries are compressed during ventricular systole as in the reference model (Zinemanas et al. 1994), and the model produces coronary arterial backflow during ventricular contraction. However, we simplified the present model to omit intramyocardial venules; the coronary veins are considered to lie on the epicardial surface, not subject to systolic compression.

Subject-specific Parameterization

The automated parameterization method was successful in precisely tuning a lumped-parameter, closed-loop circulatory system and its baroreceptor control to match the hemodynamic measurements listed in Table 7 for each animal. However, in some animals there was a tendency for the optimization to converge toward erroneously low estimates of aortic compliance and volume. The low compliance reduces the Windkessel effect and increases the range of peak values of systolic forward flow, though it does not change the estimated CO. However, in those animals with aortic compliances that were tuned low, TBV was likely slightly underestimated.

Cardiac Output Estimation

As shown in Table 5 and the Bland-Altman bias of the grouped CO data in Fig. 4 it appears the model modestly underestimates CO. The magnitude of the offset is similar to that observed in other CO estimation methods that rely on pulse-contour analyses of the arterial blood pressure waveform reported by Goedje et al. (1999), Jansen et al.

(uncalibrated) (2001), and Wesseling et al. (cZ method) (1993). However, some other pulse contour techniques report better accuracy [Hamilton 2002; calibrated Jansen 2001; Redling and Akay 1997; Rodig et al. 1999; Scoletta 2005; Wesseling et al. 1993 (model flow method)]. The overall limits of agreement of the Bland-Altman analysis in Fig. 4 (the boundaries that include 95% of the data points around the mean) are tighter than or comparable to the limits of agreement in many of these studies [Goedje et al. 1999; Hamilton 2002; Jansen 2001; Redling and Akay 1997; Rodig et al. 1999; Wesseling et al. 1993 (cZ method)]. This suggests the present method may better account for physiological variability between subjects.

Pulse contour techniques rely on high fidelity in recording the systemic pressure signal and make use of the geometric and physical properties of the arterial network. The major difficulty with many of these techniques is their need for excellent quality in the recorded ABP curve, requiring intravascular pressure to be obtained by catheter or direct needle puncture. In contrast, our approach allows the use of crude or low fidelity pressure data to generate CO estimates, since ABP waveform analysis is not required. Our model could estimate CO from *non-invasive* blood pressure cuff measurements given a formula for estimating MAP from ABP_S and ABP_D. The operational principle here is that model complexity and robustness can compensate for high fidelity in data acquisition in providing good estimates of hemodynamics.

In the open-loop CO estimation model, the accuracy of the CO estimate depends greatly on the model's estimated total peripheral resistance (TPR), since CO is adjusted to match the model and measured MAP. This is simply Ohm's law (Eq. 2): Flow through the peripheral circulation is equal to the pressure drop across the peripheral circulation (MAP − EDP_{RV}) divided by the model-estimated TPR. Therefore, inaccuracies in TPR estimation will directly affect CO estimates. This becomes important as hypovolemia and arterial pressure loss are compensated for by an increase in arteriolar resistance induced by the baroreceptor response. Thus, the baroreceptor equations, which raise systemic arteriolar resistance with decreases in arterial blood pressure, are critical to the accuracy of CO estimation. The model's baroreceptor responses are not well defined for each animal since the baseline data were in steady state and the same baroreceptor parameters were used for all animals. This weakness could be overcome if a subject's characteristic vascular response to changes in central blood pressure could be ascertained prior to injury, such as through a head-up tilt, Valsalva maneuver, or lower body negative pressure test. Thus, the accuracy of ABP-derived, noninvasive CO estimation will certainly be improved if each subject's baroreceptor-mediated responses are gauged.

Total Blood Volume Estimation

Although we do not have a set of true blood volumes against which to assess model estimates of TBV, the results in Fig. 5A reveal a distinct cut-off separating surviving animals from nonsurvivors: pigs that lost more than 45% of their initial blood volume following hemorrhage did not survive the 2-h post-injury observation period, and no surviving pigs lost more than 28% of estimated TBV. This separation between the two groups corresponds to clinical classification of hemorrhage severity based on percent TBV lost: a loss of 40% or more portends cardiovascular collapse (Marino 1998). If further validation supports this distinction between survivors and nonsurvivors, model TBV estimates may prove useful as an aid in triage and emergency care.

The CO estimation model also provides estimates of TBV without using the flowmeter data as input. While there were differences between the blood losses estimated by the two open-loop models (Fig. 5), the differences between surviving and nonsurviving pigs were significant using either open-loop model form, and the boundaries for survivability were nearly the same in both sets of results. Using the CO estimation model (based only on ABP and HR), estimated maximum blood loss of the surviving group was 29% and minimum blood loss among nonsurvivors was estimated at 45%.

Model TBV estimates depend on compliances throughout the circulation. During sympathetic activation, these compliances shift to increase venous return and ensure metabolic supply to the central organs. While our models account for compliance changes at the arteriolar level due to sympathetic outflow, the modeled venous compliances are not baroreceptor-dependent. Therefore, the accuracy of TBV estimates would likely benefit from empirically based individuation of the model's venous response to sympathetic stimulation.

Model Limitations

In the late phase of each animal experiment, as the hemorrhage causes the ABP to drop, the arteriolar resistance in the model remains activated as if the sympathetic vasoconstriction continued. Therefore, estimates of CO near the point of death will be inaccurate if the subject's arteriolar resistance and/or venous tone decrease as efferent neural firing and smooth muscle metabolism drop due to lack of oxygen. Changes in cardiac contractility that might occur with lowered blood pressure and reduced coronary flow are not accounted for either: the maximal ventricular elastances are not reduced as coronary perfusion pressure falls. This may be the reason

why CO is overestimated near death in the nonsurviving subjects (refer to values after 32 min for animal P132 in Fig. 3A), and why subjects that died relatively quickly following injury (for example, P80, P179, P193, and P198) have positive CO biases. In nonsurviving animals, end-diastolic ventricular pressures drop immediately following injury (presumably due to loss of circulating blood volume) then usually rise in the minutes preceding death. This rise suggests a near-death diminution in contractile force development and ventricular ejection fraction. Assuming an accurate TPR estimate, the model will predict an overly high value for CO when EDP_{RV} increases due to contractility loss, since the downstream pressure of the peripheral circulation in the model is lower than the measured value. In a similar way, increased venous compliance from loss of smooth muscle tone may also contribute to CO overestimation near death. Venous pressures predicted by the model would also be lower than actual values if there were significant pooling in the subject's venous system following hemorrhage.

The simplification of the vascular PV relationships worked well for the arterial system but introduces a problem in correctly representing cardiac chamber volumes: the result of not having a concave-upward PV curve for the ventricles means that atrial contraction contributes too much additional volume to the ventricles at the end of diastole. To compensate for this, the atrial systolic elastances are reduced and the atrial volume fluctuations are lower than in real life in order to allow correct behavior in the rest of the model.

Medical Applicability

Next-generation triage methods using automated, digitized vital sign collection, hand-held computing systems, and wireless data networking are being developed and field-tested in mass-casualty simulations (Chan et al. 2004; Gao 2006; Gao et al. 2005, 2006; Killeen et al. 2006; Massey et al. 2006). These new systems allow first responders to collect HR and ABP data from trauma victims by applying ECG leads and automated blood pressure cuffs that transmit data over wireless network connections to hand-held computers. These measurements are then integrated with other patient data at the site of care (Gao et al. 2006). Since the model presented in detail here is capable of providing surrogate hemodynamic measurements from HR and ABP given a subject's baseline (pre-injury) parameter set, we envision it functioning in concert with these new triage methods to provide medics with a more complete hemodynamic assessment of individual casualties. A more thorough

hemodynamic profile may then improve the effectiveness of triage decision-making, although further study will be required to confirm this.

An individual's baseline parameterization data must be accessible to the medic at the point of care in order to estimate hemodynamics post-injury. These parameters must be read in to the open-loop models before results can be provided. We therefore see the most immediate application of this modeling technology in military field medicine, where electronic dog tags containing an individual soldier's medical data are already in use. An individual's baseline parameter set could easily be stored and accessed using such a device, given the low memory requirements. Eventually, however, it may be practical to compute and store baseline parameter sets for civilians working in high-risk occupations so that model-estimated hemodynamics could be generated following trauma. Patient data might then be carried in a form similar to a dog tag, but given that networked barcode scanners are also part of the new triage tools under development (Killeen et al. 2006), bar-coded information on individual identification cards, bracelets, etc. could also be scanned in and used to retrieve patient parameters from a centralized repository.

Appendix

Equations of the Open-loop Cardiac Output Estimation Model

Lower-case subscript key:

0: unstressed volume
a: left or right atrium
d: diastolic
h: circulatory segment immediately upstream of the i segment
i: left atrium, left ventricle, right atrium or right ventricle
j: circulatory segment immediately downstream of the i segment
s: systolic
v: left or right ventricle

Four-chamber Heart

Heart chamber activation function

$$y_i = \begin{cases} \dfrac{1.0 - \cos\dfrac{\pi \times t_{i,REL}}{Ts_i}}{2.0} & \text{for } (0, 0 \leq t_{i,REL} < TS_i) \\[2ex] \dfrac{1.0 + \cos[2.0 \times \pi \times (t_{i,REL} - Ts_i)]}{2.0} & \text{for } (Ts_i \leq t_{i,REL} \\ & \quad < 1.5 \times Ts_i) \\[1ex] 0 & \text{for } (t_{i,REL} \geq 1.5 \times Ts_i) \end{cases} \quad \text{(A.1)}$$

$$t_{a,REL} = t - t_{PWAVE} \tag{A.2}$$

$$t_{v,REL} = t - t_{RWAVE} \tag{A.3}$$

Discrete functions to set heart beat start time and heart period

In the model the x domain was created as the set of all positive integers, and used to access R wave event times and heart periods indexed by heartbeat number in an external data file created from empirical ECG data. The functions m and n increased by 1 after each heart cycle completed, and t_{HB} was set to the R wave event time for each heartbeat. The heart period HP was also set discretely for each indexed heartbeat.

$$m = m(x) \tag{A.4}$$

$$n = n(x) \tag{A.5}$$

$$t_{HB} = t_{HB}(x) \tag{A.6}$$

$$HP = HP(x) \tag{A.7}$$

for $(t \geq t_{HB}(n + 1) - PR_{INT} - offv)\{$

$$HR_a = \frac{1}{HP(m + 1)} \tag{A.8}$$

$$Ts_a = Ts1_a \times \sqrt{Ts2/HR_a} \tag{A.9}$$

$$t_{PWAVE} = t_{HB}(n + 1) - PR_{INT} - offv \tag{A.10}$$

$$n = n + 1\} \tag{A.11}$$

for $(t \geq t_{HB}(m + 1) - offv)\{$

$$HR_v = \frac{1}{HP(m + 1)} \tag{A.12}$$

$$Ts_v = Ts1_v \times \sqrt{Ts2/HR_v} \tag{A.13}$$

$$t_{\text{RWAVE}} = t_{\text{HB}}(m+1) - offv \qquad (A.14)$$

$$m = n \qquad (A.15)$$

$$Vvar_{\text{vs0}} = \begin{array}{ll} V_{\text{vd0}} & \text{for} \, (V_v < V_{\text{vd0}}) \\ V_{\text{vs0}} & \text{for} \, (V_v > \text{EDV}_v) \\ \dfrac{(V_{vs0} - V_{\text{vd0}}) \times (V_v - V_{\text{vd0}})}{(\text{EDV}_v - V_{\text{vd0}})} \\ \quad + V_{\text{vd0}} & \text{for} \, V_{\text{vd0}} \le V_v \le \text{EDV}_v \end{array} \qquad (A.16)$$

$$af_{\text{CON2}} = af_{\text{CON}}\} \qquad (A.17)$$

$$\text{HR} = \text{HR}_v \qquad (A.18)$$

Heart chamber pressure-volume relationships

$$P_v = E_v \times (V_v - V_{v0}) \times af_{\text{CON2}} - \Psi \qquad (A.19)$$

$$P_a = E_a \times (V_a - V_{a0}) - \Psi \qquad (A.20)$$

$$E_i = y_i \times (E_{\text{MAX,i}} - E_{\text{MIN,i}}) + E_{\text{MIN,i}} \qquad (A.21)$$

$$E_{\text{MAX,v}} = \text{KE}_v \times E_{\text{MAX,v1}} \qquad (A.22)$$

$$V_{v0} = (1 - y_v) \times (V_{\text{vd0}} - Vvar_{\text{vs0}}) + Vvar_{\text{vs0}} \qquad (A.23)$$

$$V_{a0} = (1 - y_a) \times (V_{\text{ad0}} - V_{\text{as0}}) + V_{\text{as0}} \qquad (A.24)$$

Heart chamber flows

$$F_i = \begin{array}{ll} \frac{P_i - P_j}{R_i} & \text{for} \, (P_i > P_j) \\ 0 & \text{for} \, (P_i \le P_j) \end{array} \qquad (A.25)$$

$$\frac{\text{d}V_i}{\text{d}t} = F_h - F_i \qquad (A.26)$$

Systemic Circulation

Aortic flow estimate

$$\frac{\text{d}\text{AOF}_{\text{MOD}}}{\text{d}t} = (\text{MAP}_{\text{MEAS}} - \text{MAP}_{\text{MOD}}) \times K_{\text{CO,MAP}} \qquad (A.27)$$

Smoothed pulmonary valve flow

$$F_{\text{RV,SM}} = \frac{F_{\text{RV}} - F_{\text{RV,SM}}}{\tau_{\text{CO}}} \qquad (A.28)$$

Cardiac output estimate

$$\text{CO}_{\text{MOD}} = F_{\text{RV,SM}} \qquad (A.29)$$

Stroke volume

$$\text{SV} = \text{CO}_{\text{MOD}} \times \text{HR} \qquad (A.30)$$

Time-shifted, measured arterial blood pressure

$$\text{ABP}_{\text{SHIFT}} = \text{ABP}_{\text{MEAS}}(t + offv) \qquad (A.31)$$

Approximate "derivative" of arterial blood pressure, produced using a lag operator with a small time constant

$$\frac{\text{d}\text{ABP}_{\text{FOL}}}{\text{d}t} = \frac{\text{ABP}_{\text{SHIFT}} - \text{ABP}_{\text{FOL}}}{\tau_{\text{ABP}}} \qquad (A.32)$$

Tuned scaling factor for systemic veins PV relationship

$$K_V = K_{\text{V1}} \times K_{\text{SV}} \qquad (A.33)$$

Aortic afterload set by time-shifted arterial blood pressure data

$$P_{\text{AOD}} = \text{ABP}_{\text{SHIFT}} \qquad (A.34)$$

Systemic circulation pressures

$$\frac{\text{d}P_{\text{AOP}}}{\text{d}t} = \frac{F_{\text{LV}} - \frac{\text{d}V_{\text{AOP}}}{\text{d}t} - F_{\text{AOP}} - F_{\text{CORAO}}}{C_{\text{CORAO}}} \qquad (A.35)$$

$$\text{MAP}_{\text{MOD}} = \frac{R_{\text{CRB}} \times (R_{\text{TAOD}} \times \text{AOF}_{\text{MOD}}) - (F_{\text{AOD}} \times R_{\text{TAOD}}) + \frac{V_{\text{AOD}} - V_{\text{AOD,0}}}{C_{\text{AOD}}} - \Psi + (P_{\text{VC}} \times R_{\text{TAOD}})}{R_{\text{CRB}} + R_{\text{TAOD}}} \qquad (A.36)$$

$$P_{\text{SAP}} = (V_{\text{SAP}} - V_{\text{SAP,0}})/C_{\text{SAP}} - \Psi \qquad (A.37)$$

Ψ is given by $\Psi = K_{\text{XP}}/e^{v/k_{\text{XV}}} - 1)$ where V is volume and K_{XP} and K_{XV} are curve-shaping constants (see Table 3).

$$P_{\text{SA,A}} = Kc \times \log\left[\frac{V_{\text{SA}} - V_{\text{SA,0}}}{D_0} + 1\right] \qquad (A.38)$$

$$P_{\text{SA,P}} = Kp1 \times e^{[\tau_{\text{P}} \times (V_{\text{SA}} - V_{\text{SA,0}})]} + Kp2 \times (V_{\text{SA}} - V_{\text{SA,0}})^2 \qquad (A.39)$$

$$P_{SA} = (f_{VASO} \times P_{SA,A}) + [(1 - f_{VASO}) \times P_{SA,P}] \quad (A.40)$$

$$P_{SC} = (V_{SC} - V_{SC,0})/C_{SC} - \Psi \quad (A,41)$$

$$P_{SV} = -K_V \times \log\left[\frac{V_{MAX,SV}}{V_{SV}} - 0.99\right] \quad (A.42)$$

$$P_{VC} = \begin{array}{ll} K1 \times (V_{VC} - V_0) - \Psi & \text{for } (V_{VC} > V_0) \\ D2 + \left[K2 \times e^{\frac{V_{VC}}{V_{MIN,VC}}}\right] - \Psi & \text{for } (V_{VC} \le V_0) \end{array} \quad (A.43)$$

Systemic circulation forward flow

$$\frac{dF_{AOP}}{dt} = \frac{P_{AOP} - (F_{AOP} \times R_{AOP}) - ABP_{MEAS}}{L_{AOP}} \quad (A.44)$$

$$\frac{dF_{AOD}}{dt} = \frac{MAP_{MOD} - (F_{AOD} \times R_{AOD}) - P_{SAP}}{L_{AOD}} \quad (A.45)$$

$$F_{CRB} = (MAP_{MOD} - P_{VC})/R_{CRB} \quad (A.46)$$

$$F_{SAP} = (P_{SAP} - P_{SA})/R_{SAP} \quad (A.47)$$

$$F_{SA} = (P_{SA} - P_{SC})/R_{SA} \quad (A.48)$$

$$F_{SC} = (P_{SC} - P_{SV})/R_{SC} \quad (A.49)$$

$$\frac{dV_{SA}}{dt} = F_{SAP} - F_{SA} \quad (A.54)$$

$$\frac{dV_{SAP}}{dt} = F_{AOD} - F_{SAP} \quad (A.55)$$

$$\frac{dV_{SC}}{dt} = F_{SA} - F_{SC} \quad (A.56)$$

$$\frac{dV_{SV}}{dt} = F_{SC} - F_{SV} \quad (A.57)$$

$$\frac{dV_{VC}}{dt} = F_{SV} - F_{CRB} - F_{VC} \quad (A.58)$$

Nonlinear systemic resistances

$$R_{SA} = [Kr \times e^{(4 \times f_{VASO})}] + \left[Kr + \frac{V_{SA,MAX}^2}{V_{SA}}\right] + R_{SA0} \quad (A.59)$$

$$R_{VC} = \left[KR \times \frac{V_{MAX,VC}^2}{V_{VC}}\right] + R_0 \quad (A.60)$$

Pulmonary Circulation

Pulmonary circulation pressures

$$P_{PAP} = \begin{array}{ll} \dfrac{(R_{TPAP} \times P_{RV}) - (R_{PUV} \times F_{PAP} \times R_{TPAP}) + \left[R_{PUV} \times \frac{V_{PAP} - V_{PAP,0}}{C_{PAP}} - \Psi\right]}{R_{TPAP} + R_{PUV}} & \text{for } (P_{LV} > P_{PAP}) \\[3ex] \dfrac{\left[R_{PUV} \times \frac{V_{PAP} - V_{PAP,0}}{C_{PAP}} - \Psi\right](R_{PUV} \times F_{PAP} \times R_{TPAP})}{R_{PUV}} & \text{for } (P_{PAP} \le P_{LV}) \end{array} \quad (A.61)$$

$$F_{SV} = (P_{SV} - P_{VC})/R_{SV} \quad (A.50)$$

$$F_{VC} = (P_{VC} - P_{RA})/R_{VC} \quad (A.51)$$

Systemic circulation radial flow

$$\frac{dV_{AOP}}{dt} = \frac{P_{AOP} - \frac{V_{AOP} - V_{AOP,0}}{c_{AOP}}}{R_{TAOP}} \quad (A.52)$$

$$\frac{dV_{AOP}}{dt} = AOF_{MOD} - F_{AOD} - F_{CRB} \quad (A.53)$$

$$P_{PAP} = (F_{PAP} \times R_{TPAD}) - (F_{PAD} \times R_{TPAD}) + \frac{V_{PAD} - V_{PAD,0}}{C_{PAD}} - \Psi \quad (A.62)$$

$$P_{PA} = (V_{PA} - V_{PA,0})/C_{PA} - \Psi \quad (A.63)$$

$$P_{PC} = (V_{PC} - V_{PC,0})/C_{PC} - \Psi \quad (A.64)$$

$$P_{PV} = (V_{PV} - V_{PV,0})/C_{PV} - \Psi \quad (A.65)$$

Pulmonary circulation forward flows

$$F_{PS} = (P_{PA} - P_{PV})/R_{PS} \tag{A.66}$$

$$F_{PA} = (P_{PA} - P_{PC})/R_{PA} \tag{A.67}$$

$$F_{PC} = (P_{PC} - P_{PV})/R_{PC} \tag{A.68}$$

$$F_{PV} = (P_{PV} - P_{LA})/R_{PV} \tag{A.69}$$

Pulmonary circulation radial flows

$$\frac{dV_{PAD}}{dt} = F_{PAP} - F_{PAD} \tag{A.70}$$

$$\frac{dV_{PAP}}{dt} = F_{RV} - F_{PAP} \tag{A.71}$$

$$\frac{dV_{PAD}}{dt} = F_{PAP} - F_{PAD} \tag{A.72}$$

$$\frac{dV_{PA}}{dt} = F_{PAD} - F_{PS} - F_{PA} \tag{A.73}$$

$$\frac{dV_{PC}}{dt} = F_{PA} - F_{PC} \tag{A.74}$$

$$\frac{dV_{PV}}{dt} = F_{PC} + F_{PS} - F_{PV} \tag{A.75}$$

$$\frac{dF_{PAP}}{dt} = \frac{P_{PAP} - P_{PAD} - (F_{PAP} \times R_{PAP})}{L_{PAP}} \tag{A.76}$$

$$\frac{dF_{PAD}}{dt} = \frac{P_{PAD} - P_{PA} - (F_{PAD} \times R_{PAD})}{L_{PAD}} \tag{A.77}$$

Coronary Circulation

Coronary circulation pressures

$$P_{COREPI} = P_{AOP} \tag{A.78}$$

$$P_{CORINTRA} = (V_{CORINTRA} - V_{CORINTRA,0})/C_{CORINTRA} - \Psi \tag{A.79}$$

$$P_{CORCAP} = (V_{CORCAP} - V_{CORCAP,0})/C_{CORCAP} - \Psi \tag{A.80}$$

$$P_{CORVN} = (V_{CORVN} - V_{CORVN,0})/C_{CORVN} - \Psi \tag{A.81}$$

$$P_{CORINTRA,C} = V_{CORINTRA} + P_{IM} \tag{A.82}$$

$$P_{CORCAP,C} = V_{CORCAP} + P_{IM} \tag{A.83}$$

$$P_{CORVN,C} = P_{CORVN} \tag{A.84}$$

$$P_{IM} = |P_{LV}/2| \tag{A.85}$$

Coronary circulation flows

$$F_{COREPI} = (P_{COREPI} - P_{CORINTRA,C})/R_{COREPI} \tag{A.86}$$

$$F_{CORINTRA} = (P_{CORINTRA,C} - P_{CORCAP,C})/R_{CORINTRA} \tag{A.87}$$

$$F_{CORCAP} = (P_{CORCAP,C} - P_{CORVN,C})/R_{CORCAP} \tag{A.88}$$

$$F_{CORVN} = (P_{CORVN,C} - P_{RA})/R_{CORVN} \tag{A.89}$$

$$\frac{dV_{COREPI}}{dt} = F_{LV} - \frac{dV_{AOP}}{dt} - F_{AOP} - F_{COREPI} \tag{A.90}$$

$$\frac{dV_{CORINTRA}}{dt} = F_{COREPI} - F_{CORINTRA} \tag{A.91}$$

$$\frac{dV_{CORCAP}}{dt} = F_{CORINTRA} - F_{CORCAP} \tag{A.92}$$

$$\frac{dV_{CORVN}}{dt} = F_{CORCAP} - F_{CORVN} \tag{A.93}$$

Baroreceptor

Transfer function for carotid sinus firing frequency

$$a2 \times a \times \frac{d^2}{dt}Nbr + \left[(a2 + a) \times \frac{d}{dt}Nbr\right] + Nbr = (K \times ABP_{MEAS}) + a1 \times K \times \frac{dABP_{FOL}}{dt} \tag{A.94}$$

Equations of efferent pathways

$$\frac{dN_{CON}}{dt} = \begin{cases} \dfrac{-N_{CON}[K_{CON} \times Nbr(t - l_{CON})]}{T_{CON}} & \text{for } (t - t_{MIN} < l_{CON}) \\ 0 & \text{for } (t - t_{MIN} \geq l_{CON}) \end{cases} \tag{A.95}$$

$$\frac{dN_{VASO}}{dt} = \begin{cases} \dfrac{-N_{VASO}[K_{VASO} \times Nbr(t - l_{VASO})]}{T_{VASO}} & \text{for } (t - t_{MIN} < l_{VASO}) \\ 0 & \text{for } (t - t_{MIN} \geq l_{VASO}) \end{cases} \tag{A.96}$$

$$f_{CON} = a_{CON} + \frac{b_{CON}}{e^{\tau_{CON} \times (N_{CON} - No_{CON})} + 1} \tag{A.97}$$

$$f_{VASO} = a_{VASO} + \frac{b_{VASO}}{e^{\tau_{VASO} \times (N_{VASO} - No_{VASO})} + 1} \tag{A.98}$$

$$b_{VASO} = 1 - a_{VASO} \tag{A.99}$$

$$af_{CON} = a_{MIN} + (Ka \times f_{CON}) \tag{A.100}$$

Blood Volumes

Total blood volume

$$TBV = V_{HEART} + V_{SYSART} + V_{SC} + V_{SYSVEN}$$
$$+ V_{PULART} + V_{PC} + V_{PV} \tag{A.101}$$

Blood volume in heart

$$V_{HEART} = V_{RA} + V_{RV} + V_{LA} + V_{LV} + V_{CORCIRC} \tag{A.102}$$

Blood volume in coronary circulation

$$V_{CORCIRC} = V_{COREPI} + V_{CORINTRA} + V_{CORCAP} + V_{CORVN} \tag{A.103}$$

Blood volume in systemic arterial system

$$V_{SYSART} = V_{AOP} + V_{AOD} + V_{SAP} + V_{SA} \tag{A.104}$$

Blood volume in systemic venous system

$$V_{SYSVEN} = V_{SV} + V_{VC} \tag{A.105}$$

Blood volume in pulmonary arterial system

$$V_{PULART} = V_{PAP} + V_{PAD} + V_{PA} \tag{A.106}$$

References

Altman PL, Dittmer DS, editors. Respiration and circulation. Bethesda, Maryland: Federation of American Societies for Experimental Biology; 1971. 930 pp.

Athanasiades A, Ghorbel F, Clark JW Jr, Niranjan SC, Olansen J, Zwischenberger JB, Bidani A. Energy analysis of a nonlinear model of the normal human lung. J Biol Syst 2000;8:115–39.

Avolio AP. Multi-branched model of the human arterial system. Med Biol Eng Comput 1980;18:709–18.

Bland JM, Altman DG. Statistical methods for assessing agreement between two methods of clinical measurement. Lancet 1986;8:307–10.

Bourgeois MJ, Gilbert BK, Von Bernuth G, Wood EH. Continuous determination of beat to beat stroke volume from aortic pressure pulses in the dog. Circ Res 1976;39:15–24.

Chan TC, Killeen J, Griswold W, Lenert L. Information technology and emergency medical care during disasters. Acad Emerg Med 2004;11:1229–36.

Cohen SD, Hindmarsh AC. CVODE, a stiff/nonstiff ODE solver in C. Comput Phys 1996;10:138–43.

Dash RK, Bassingthwaighte JB. Blood HbO$_2$ and HbCO$_2$ dissociation curves at varied O$_2$, CO$_2$, pH, 2,3-DPG and temperature levels. Ann Biomed Eng 2004;32:1676–93.

Dash RK, Li Z, Bassingthwaighte JB. Simultaneous blood-tissue exchange of oxygen, carbon dioxide, bicarbonate, and hydrogen ion. Ann Biomed Eng 2006;34:1129–48.

Drzewiecki G, Field S, Moubarak I, Li JK-J. Vessel growth and collapsible pressure-area relationship. Am J Physiol Heart Circ Physiol 1997;273:H2030–43.

Feigl EO. Coronary circulation. In: Patton HD, Fuchs AF, Hille B, Scher AM, Steiner R, editors. Textbook of physiology. Philadelphia, PA: W. B. Saunders; 1989. p. 933–951.

Gao T. Lessons learned from mass casualty drill at Maryland Fire and Rescue Institute. Johns Hopkins University Applied Physics Laboratory: Internal Memo, Laurel, MD: May 11; 2006. p. 1.

Gao T, Greenspan D, Welsh M, Juang RR, Alm A. Vital signs monitoring and patient tracking over a wireless network. In: Proceedings of the 27th Annual International Conference of the IEEE EMBS. p. 1–4, September 2005.

Gao T, Kim MI, White D, Alm AM. Iterative user-centered design of a next generation patient monitoring system for emergency medical response. American Medical Informatics Association 2006 Annual Symposium Proceedings (CD-ROM). p. 284–288, November 2006.

Goedje O, Hoeke K, Lichtwarck-Aschoff M, Faltchauser A, Lamm P, Reichart B. Continuous cardiac output by femoral arterial thermodilution calibrated pulse contour analysis: comparison with pulmonary arterial thermodilution. Crit Care Med 1999;27:2407–12.

Hamilton TT, Huber LM, Jessen ME. PulseCO: a less-invasive method to monitor cardiac output from arterial pressure after cardiac surgery. Ann Thorac Surg 2002;74:S1408–12.

Heldt T, Shim EB, Kamm RD, Mark RG. Computational modeling of cardiovascular response to orthostatic stress. J Appl Physiol 2002;92:1239–54.

International Commission on Radiological Protection. Basic anatomical and physiological data for use in radiological protection: reference values. New York: Elsevier Science; 2003. p. 320.

Jansen JRC, Schreuder JJ, Mulier JP, Smith NT, Settels JJ, Wesseling KH. A comparison of cardiac output derived from the arterial pressure wave against thermodilution in cardiac surgery patients. Br J Anaesth 2001;87:212–22.

Kassab G, Lin DH, Fung Y-CB. Morphometry of pig coronary venous system. Am J Physiol 1994;267(Heart Circ Physiol 36):H2100–13.

Kassab GS, Rider CA, Tang NJ, Fung Y-CB. Morphometry of pig coronary arterial trees. Am J Physiol Heart Circ Physiol 1993;265:H350–65.

Killeen JP, Chan TC, Buono C, Griswold WG, Lenert LA. A wireless first responder handheld device for rapid triage, patient assessment and documentation during mass casualty incidents. American Medical Informatics Association 2006 Annual Symposium Proceedings (CD-ROM). p. 429–433. November 2006.

Klotz S, Hay I, Dickstein ML, Yi G-H, Wang J, Maurer M, Kass DA, Burkhoff D. Single beat estimation of the end-diastolic pressure-volume relationship: a novel method with the potential for noninvasive application. Am J Physiol Heart Circ Physiol 10.1152/ajpheart.01240.2005, January 20, 2006.

Kouchoukos NT, Sheppard LC, McDonald DA. Estimation of stroke volume in the dog by a pulse contour method. Circ Res 1970;26:611–23.

Linton NWF, Linton RAF. Estimation of changes in cardiac output from the arterial blood pressure waveform in the upper limb. Br J Anaesth 2001;86:486–96.

Lu K, Clark JW Jr, Ghorbel FH, Ware DL, Bidani A. A human cardiopulmonary system model applied to the analysis of the Valsalva maneuver. Am J Physiol Heart Circ Physiol 2001;281:H2661–79.

Lu K, Clark JW Jr, Ghorbel FH, Ware DL, Zwischenberger JB, Bidani A. Whole-body gas exchange in human predicted by a cardiopulmonary model. Cardiovasc Eng 2002;3:1–19.

Marino PL. The ICU book. Williams & Wilkins, Baltimore; 1998. p. 928.

Massey T, Gao T, Welsh M, Sharp JH, Sarrafzadeh M. The design of a decentralized electronic triage system. American Medical Informatics Association 2006 Annual Symposium Proceedings (CD-ROM). p. 544–548, November 2006.

McCombie DB, Reisner AT, Asada HH. Laguerre-model blind system identification: cardiovascular dynamics estimated from multiple peripheral circulatory signals. IEEE Trans Biomed Eng 2005;52:1889–901.

Milnor WR. Hemodynamics. Baltimore: Williams and Wilkins; 1982. p. 390.

Mohrman DE, Heller LJ. Cardiovascular physiology. 5th ed. New York McGraw-Hill; 2003. p. 257.

Nelder JA, Mead R. A simplex method for function minimization. Comput J 1965;7:308–13.

Olansen JB, Clark JW, Khoury D, Ghorbel F, Bidani A. A closed-loop model of the canine cardiovascular system that includes ventricular interaction. Comp Biomed Res 2000;33:260–95.

Redling JD, Akay M. Noninvasive cardiac output estimation: a preliminary study. Biol Cybern 1997;77:111–22.

Rideout VC. Mathematical computer modeling of physiological systems. Englewood Cliffs, NJ: Prentice Hall; 1991. p . 261.

Rödig G, Prasser C, Keyl C, Liebold A, Hobbhahn J. Continuous cardiac output measurement: pulse contour analysis vs. thermodilution technique in cardiac surgical patients. Brit J Anaesth 1999;82:525–30.

Romano SM, Pistolesi M. Assessment of cardiac output from systemic arterial pressure in humans. Crit Care Med 2002;30:1834–41.

Rosse C, Gaddum-Rosse P. Hollinshead's textbook of anatomy. 5th ed. Lippincott-Raven, Philadelphia; 1997. p. 902.

Saeed M, Mark RG. Multiparameter trend monitoring and intelligent displays using wavelet analysis. Comp Cardiol 2000;27:797–800.

Sagawa K, Lie RK, Schaefer J. Translation of Otto Frank's Paper "Die Grundform des Arteriellen Pulses" Zeitschrift für Biologie 37: 483–526 (1899). J Mol Cell Cardiol 1990;22:253–77.

Scher AM. Events of the cardiac cycle: measurements of pressure, flow and volume. In: Patton HD, Fuchs AF, Hille B, Scher AM, Steiner R, edotors. Textbook of physiology, vol. 2. Philadelphia: W. B. Saunders; 1989. p. 834–47.

Scoletta S, Romano SM, Biagioli B, Capannini G, Giomarelli P. Pressure recording analytical method (PRAM) for measurement of cardiac output during various haemodynamic states. Br J Anaeth 2005;95:159–65.

Spickler JW, Kezdi P, Geller E. Transfer characteristics of the carotid sinus pressure control system. In: Kezdi P, editor. Baroreceptors and hypertension. Dayton: Pergamon; 1967. p. 31–40.

Sun Y, Beshara M, Lucariello RJ, and Chiaramida SA. A comprehensive model for right-left heart interaction under the influence of pericardium and baroreflex. Am J Physiol Heart Circ Physiol 1997;272:H1499–515.

Toyota E, Fujimoto K, Ogasawara Y, Kajita T, Shigeto F, Matsumoto T, Goto M, Kajiya F. Dynamic changes in three-dimensional architecture and vascular volume of transmural coronary microvasculature between diastolic- and systolic-arrested rat hearts. Circulation 2002;105:621–6

Warner HR, Swan HJC, Connolly DC, Tompkins RG, Wood EH. Quantitation of beat-to-beat changes in stroke volume from the aortic pulse contour in man. J Appl Physiol 1953;5:495–507.

Wesseling KH, Jansen JRC, Settels JJ, Schreuder JJ. Computation of aortic flow from pressure in humans using a nonlinear, three-element model. J Appl Physiol 1993;74:2566–73

Wesseling KH, Settels JJ. Circulatory model of baro- and cardio-pulmonary reflexes. In: Di Rienzo M, edotor. Blood pressure and heart rate variability. IOS Press; 1992. p. 56–67.

Zinemanas D, Beyar R, Sideman S. Relating mechanics, blood flow and mass transport in the cardiac muscle. Int J Heat Mass Trans 1994;37(Suppl. 1):191–205.